Return to
TECHNICAL LIBRARY

IDO-17065
June 1965

729451

R

POST-TEST PHYSICAL, CHEMICAL AND METALLURGICAL ANALYSIS OF SNAPTRAN-3 FUEL

IFPL 7-29-80
P. North 10-7-82
HR Peterson 12/24

R. D. Fletcher

This report belongs to the INEL Technical Library. It has been loaned to you, and you are accountable for it. The library may recall it after two weeks for use by another employee. Please return this report to the library when it is recalled or when you are no longer using it.

INEL Technical Library-IF
Report Section

PHILLIPS PETROLEUM
PHILLIPS 66

REPOSITORY INEL
COLLECTION Public Reading Room
BOX No. U.S. DOE PUBLIC READING ROOM IDO UNIVERSITY PLACE
FOLDER IDO-17065

1255988

PRINTED IN USA. PRICE $3.00. AVAILABLE FROM THE CLEARINGHOUSE FOR FEDERAL SCIENTIFIC AND TECHNICAL INFORMATION, NATIONAL BUREAU OF STANDARDS, U. S. DEPARTMENT OF COMMERCE, SPRINGFIELD, VIRGINIA

LEGAL NOTICE

This report was prepared as an account of Government sponsored work. Neither the United States, nor the Commission, nor any person acting on behalf of the Commission:

A. Makes any warranty or representation, express or implied, with respect to the accuracy, completeness, or usefulness of the information contained in this report, or that the use of any information, apparatus, method, or process disclosed in this report may not infringe privately owned rights; or

B. Assumes any liabilities with respect to the use of, or for damages resulting from the use of any information, apparatus, method, or process disclosed in this report.

As used in the above, "person acting on behalf of the Commission" includes any employee or contractor of the Commission, or employee of such contractor, to the extent that such employee or contractor of the Commission, or employee of such contractor prepares, disseminates, or provides access to, any information pursuant to his employment or contract with the Commission, or his employment with such contractor.

1255989

IDO-17065
AEC Research and Development Report
Aerospace Safety
TID-4500 (40th Ed.)
Issued: June 1965

POST-TEST PHYSICAL, CHEMICAL AND METALLURGICAL ANALYSIS OF SNAPTRAN-3 FUEL

By

R. D. Fletcher

PHILLIPS
PETROLEUM
COMPANY

Atomic Energy Division
Contract AT(10-1)-205
Idaho Operations Office
U. S. ATOMIC ENERGY COMMISSION

1255990

Acknowledgment

The auther wishes to acknowledge the work of B. R. Hunter of the Analytical Chemistry Branch in the chemical analysis, and the Metallurgy and Hot Cells Branch - TAN in the recovery and metallographic examination of the fuel.

1255991

Abstract

The fuel element damage which occurred during the SNAPTRAN-3 Destructive Test of a Snap 10A/2 reactor is described. Chemical analysis of the fuel indicated that approximately 15% of the hydrogen was released and that the core flux was higher toward the center both radially and axially. Metallurgical analysis of the fuel determined the presence of the epsilon, delta, and gamma phases in the grain structure and evidence of a possible alpha or beta phase. The phase changes indicated a minimum peak fuel temperature of 1290°F while cracking at the grain boundries indicated a peak fuel temperature in excess of 1740°F. The failed edges of the fuel cladding suggested a peak clad temperature in excess of 1000°F.

1255992

TABLE OF CONTENTS

	Page No.
ACKNOWLEDGEMENT	ii
ABSTRACT	iii
I. INTRODUCTION	1
II. REACTOR DESCRIPTION	3
1. Test Package Description	3
III. OPERATION SUMMARY	7
1. Static Physics Measurement	7
2. Power Calibration	7
3. Destructive Test	7
IV. POST-DESTRUCTIVE TEST ANALYSIS	9
1. Core Inspection and Recovery	9
1.1 Core Distribution	9
1.2 Fuel Recovery and Size Distribution	9
1.3 Core Sampling	15
2. Chemical Analysis	17
2.1 Hydrogen Distribution	17
2.2 Fission Product Distribution	21
2.3 Activation Analysis	23
3. Metallurgical Examination	24
3.1 Zirconium Hydride Fuel	24
3.11 Phase Relationships	33
3.12 Microhardness	40
3.13 Cracking	41
3.14 Uranium Fuel Particles	42

1255993

TABLE OF CONTENTS (Cont.)

Page No.

3.2 Fuel Element Cladding 46

3.21 Grain Size. 46

3.22 Precipitation and Age Hardening Effects . . . 46

3.23 Cladding Failure. 51

3.24 Chromized Layer 55

3.3 Reactor Vessel Wall 55

V. CONCLUSIONS. 59

REFERENCES. 61

1255994

LIST OF FIGURES

Figure No.		Page No.
II-1	SNAPTRAN-3 Reactor and Flatcar Assembly.	4
II-2	SNAPTRAN-3 Fuel Rod	5
II-3	SNAPTRAN-3 Reactor Cross Section.	6
IV-1	Post-Test Remains of Reactor after Removal of Superstructure.	10
IV-2	Beryllium Reflectors after Destructive Test .	11
IV-3	Fuel Rod Remains Arranged According to Core Layout.	12
IV-4	Small Fuel Pieces Recovered by Vacuum Cleaning.	13
IV-5	SNAPTRAN-3 Core Layout.	16
IV-6	Cross Section 4-1/2 inches from the Bottom of Fuel Element E-65 (E-65-3).	20
IV-7	Components Examined for Activation.	25
IV-8	Upper Grid Plate Sample Locations	26
IV-9	Lower Grid Plate Sample Locations	26
IV-10	Element E-86 Cladding and Reactor Vessel Sample Locations.	27
IV-11	Neutron Activation Across Upper Grid Plate. .	27
IV-12	Neutron Activation Across Lower Grid Plate. .	28
IV-13	Neutron Activation of Element E-86 Cladding .	28
IV-14	Neutron Activation of Reactor Vessel Wall . .	28
IV-15	Radioautograph, Upper Grid Plate.	29
IV-16	Radioautograph, Lower Grid Plate.	29
IV-17	Radioautograph, E-86 Cladding	29
IV-18	Radioautograph, Reactor Vessel Wall	29
IV-19	Fuel Element Sample Locations	30

1255995

LIST OF FIGURES

Figure No.		Page No.
IV-20	Epsilon Zirconium-Hydride (Banded Grains), Element E-84, Sample R-191, Stain Etched, 500 x Magnification	35
IV-21	Epsilon (Banded Grains) plus Delta (Un-Banded Grains) Zirconium-Hydride, Element E-84, Sample R-193, Stain Etched, 500 x Magnification	35
IV-22	Gamma Zirconium-Hydride (Elongated White Particles), Element E-84, Sample R-193, Stain Etched, 500 x Magnification	36
IV-23	Delta Zirconium-Hydride (Un-Banded Grains), Unidentified Fuel Element, Sample R-192, 500 x Magnification	36
IV-24	Gamma Zirconium-Hydride (Parallel Appearing Structure Along Crack), Unidentified Fuel Element, Sample R-192, Stain Etched, 500 x Magnification	37
IV-25	Gamma Zirconium-Hydride Formation Along Cracks, Element E-65, Sample R-151, Stain Etched, 500 x Magnification	37
IV-26	Possible Beta Zirconium-Hydride (Indicated by Arrows) in Matrix of Gamma and Delta Zirconium-Hydride, Unidentified Fuel Element, Sample R-192, Stain Etched, 500 x Magnification.	38
IV-27	Small Intergranular Cracks, Element E-84, Sample R-193, as Polished, 500 x Magnification.	43
IV-28	Small Intergranular Cracks, Unidentified Fuel Element, Sample R-192, as Polished, 500 x Magnification	43
IV-29	Very Small Fuel Particles and Large Islands with Cored Area, Element E-84, Sample R-191, Etch-Polish-2 for 30 seconds, 500 x Magnification	44
IV-30	Very Small Fuel Particles and Large Islands with Light Coloring, Element E-84, Sample R-193, Etch-Polish-2 for 45 seconds, 500 x Magnification	44

1255996

LIST OF FIGURES

Figure No.		Page No.
IV-31	Very Small Fuel Particles and Large Islands with Dark Coloring, Unidentified Fuel Element, Sample R-192, Etch-Polish-2 for 30 seconds, 500 x Magnification.	45
IV-32	Very Small Fuel Particles and Large Islands with Cored Area, Element E-65, Sample R-155 Etch-Polish-2 for 16 seconds, 500 x Magnification	45
IV-33	Element E-65 Cladding Samples	47
IV-34	Element E-84 Cladding Samples	47
IV-35	Cladding Grain Structure at the Cold End of the Element, Element E-84, Sample A-175, Shantz Etch for 10 seconds, 250 x Magnification.	48
IV-36	Cladding Grain Structure at the Crack Termination Region of the Element, Element E-84, Sample A-173A, Shantz Etch for 10 seconds, 250 x Magnification	48
IV-37	Cladding Grain Structure at the Hot End of the Element, Element E-84, Sample A-173B, Shantz Etch for 10 seconds, 250 x Magnification.	49
IV-38	Cladding Grain Structure at the Cold End of the Element, Element E-65, Sample A-165A, Shantz Etch for 15 seconds, 250 x Magnification.	49
IV-39	Cladding Grain Structure at the Hot End of the Element, Element E-65, Sample A-165C, Shantz Etch for 15 seconds, 250 x Magnification.	50
IV-40	Unfailed Cladding, Element E-65, Sample R-162, as Polished, 250 x Magnification.	52
IV-41	Failed Cladding, Element E-65, Sample R-162, Schantz Etch, 250 x Magnification	52
IV-42	Unfailed Cladding, Element E-84, Sample R-163, as Polished, 250 x Magnification.	53

1255997

LIST OF FIGURES

Figure No.		Page No.
IV-43	Failed Cladding, Elemtn E-84, Sample R-163, Shantz Etch, 250 x Magnification . . .	53
IV-44	Crack Termination in Weld, Element E-65, Sample A-166, Shantz Etch, 50 x Magnification	54
IV-45	Crack Termination in Weld, Element E-84, Sample A-174, Shantz Etch, 50 x Magnification	54
IV-46	Chromized Layer on the Walls, Element E-65 Sample R-162, Shantz Etch, 250 x Magnification	56
IV-47	Chromized Layer on the Walls, Element E-65, Sample R-162, Shantz Etch, 250 x Magnification	56
IV-48	Chromized Layer on the Walls, Element E-84, Sample R-163, Shantz Etch, 250 x Magnification	57
IV-49	Reactor Vessel Wall, Typical, Sample R-178, 10% Oxalic Etchant, 500 x Magnification . . .	57
IV-50	Reactor Vessel Wall, Failed Edge, Sample R-178, 10% Oxalic Etchant, 500 x Magnification	58

1255998

TABLES

Table No.		Page No.
I.	SNAPTRAN-3 Destructive Test Nuclear Data.	8
II.	Size Analysis of Fines.	14
III.	Particle Distribution, 200 mesh	14
IV.	Sample Wafer Identification and Location. .	15
V.	Hydrogen Analysis of Fuel Wafers.	19
VI.	Spot Hydrogen Analysis and Percentage Hydrogen Loss	21
VII.	Fission Product Distribution.	22
VIII.	Metallography Samples	31
IX.	X-Ray Diffraction Data.	39
X.	Fuel Microhardness.	41
XI.	Cladding Microhardness.	50

1255999

I. INTRODUCTION

This report describes the physical, chemical, and metallurgical analysis of the SNAPTRAN-3 reactor fuel following the destructive testing of the reactor. The SNAPTRAN-3 reactor tested to destruction was a modified SNAP 10A/2 flight machine designed for the purpose of investigating the consequence of a nuclear excursion resulting from the immersion of the SNAP 10A/2 reactor core in water. This is a portion of the overall aerospace nuclear safety program that has been designated as SNAPTRAN and is being conducted by Phillips Petroleum Company at the Test Area North (TAN) site of the National Reactor Testing Station. The SNAP 10A/2 type reactors are approximately 9 inches in diameter by 12 inches long and are composed of a core containing 37 fuel rods of an alloy of zirconium-hydride and 10 wt% of 93% enriched uranium. A more complete description of the SNAPTRAN-3 reactor package and fuel is presented in Section II, "Reactor Description".

The experimental program prior to the destructive test included mechanical, electrical, and hydraulic checkout; fuel loading, static physics measurements; and a transient test. Results of the physics measurements and transient test are summarized in Section III, "Operation Summary".

Although the complete disassembly of the reactor and the dispersal of the fuel in a non-critical array was the anticipated consequence of the destructive test, the entire area was surveyed with neutron and gamma detectors and with two remotely controlled television cameras mounted above the reactor package prior to any personnel entry. A few minutes after the test it was ascertained that the reactor was shutdown and that no foreseeable event could lead to criticality.

Following the destructive test a preliminary radiation survey of the test cell area indicated that levels were sufficiently low as to permit limited personnel entry and the manual recovery of air monitoring equipment and samples. Twenty-four hours after the test a radiation survey indicated the gamma dose rate at the inner edge of the environmental tank was in agreement with the pre-test calculations of

1256000

3 rem/hour for a comparable energy release. A contamination survey of the test area also indicated that only a very small amount of fuel had escaped from the environmental tank.

The test dolly and reactor remains were transferred to the TAN Service Facilities (TSF) area hot shop for detailed examination of the reactor components and fuel one week after the destructive test.

1256001

II. REACTOR DESCRIPTION

1. Test Package Description

A pictorial representation of the SNAPTRAN-3 reactor test package prior to the destructive test is given in Figure II-1. The reactor core was mounted on a pedestal in the center of the steel lined environmental tank and was surrounded by a Binal poison sleeve. The tank was 14 feet inside diameter, 10 feet high, and filled with water to 3.5 feet above the top of the reactor core. The steel tank liner was backed by one foot of concrete at the top and two feet of concrete at the bottom to maintain the tank integrity during the destructive disassembly of the reactor. The superstructure shown above the environmental tank supported the Binal poison sleeve drive mechanism. The entire reactor assembly and environmental tank were mounted on a 4-rail dolly to facilitate movement of the test package to the Examination Area (TAN 607) following the destructive test.

The 37 fuel rods which made up the core were an alloy of zirconium-hydride and 10 wt% of 93% enriched uranium. A typical fuel rod is shown in Figure II-2. The rods were clad with 0.015 inch thick Hastelloy-N and had an outside diameter of 1.250 inches and a length of 12.25 inches. The beryllium filler pieces were used to adapt the hexagonal form of the core to the cylindrical reactor vessel. A cross section of the fuel rod arrangement, the location of the six beryllium filler pieces, the reactor vessel and the binal control sleeve are shown in Figure II-3.

The reactor vessel shown in Figure II-3 was fabricated from 0.032 inch thick type 316 stainless steel, was cylindrical in shape, and had an outside diameter of 8.94 inches. The fuel rods were positioned accurately with respect to each other and the reactor vessel by upper and lower grid plates within the vessel. The cap and grid plate indexing pins shown at opposite ends of the fuel rod in Figure II-2 engaged the Hastelloy-C grid plates for the precision positioning.

1256002

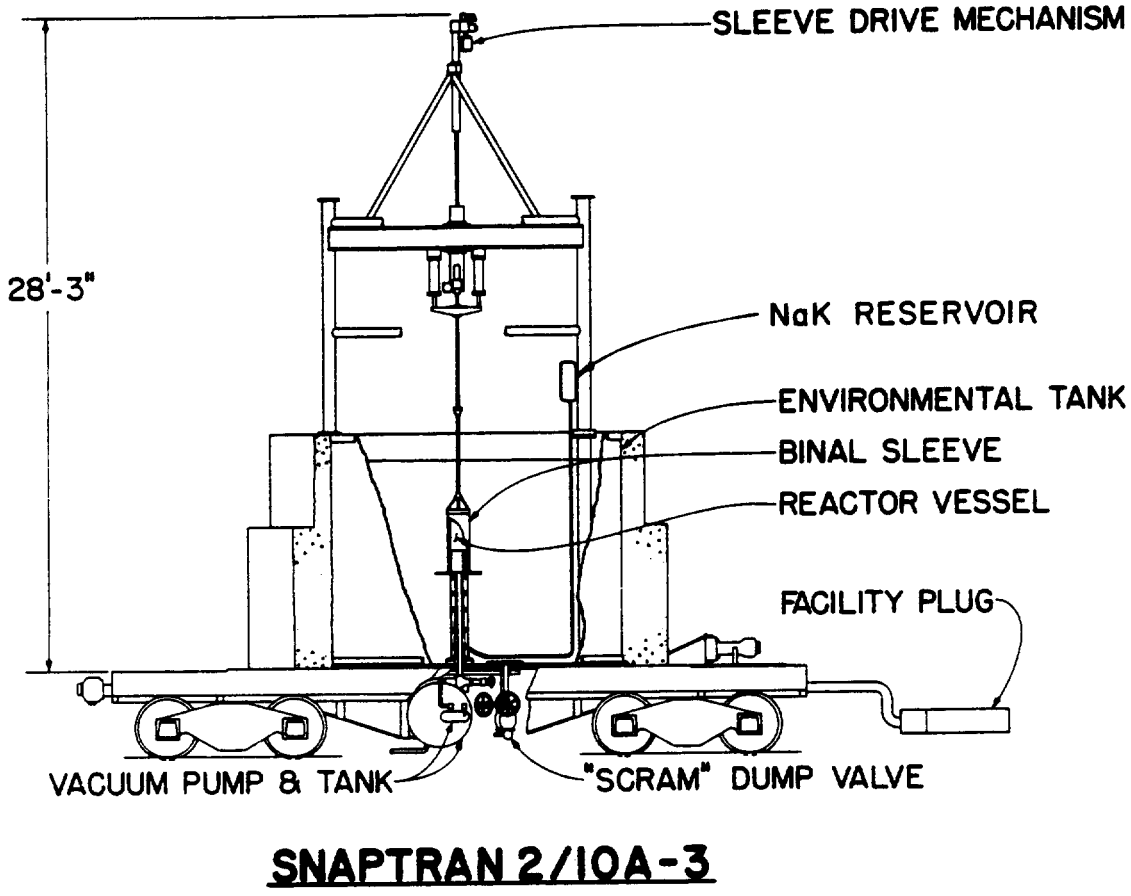

Fig. II-1 SNAPTRAN-3 Reactor and Flatcar Assembly.

1256003

Fig. II-2 SNAPTRAN-3 Fuel Rod.

1256004

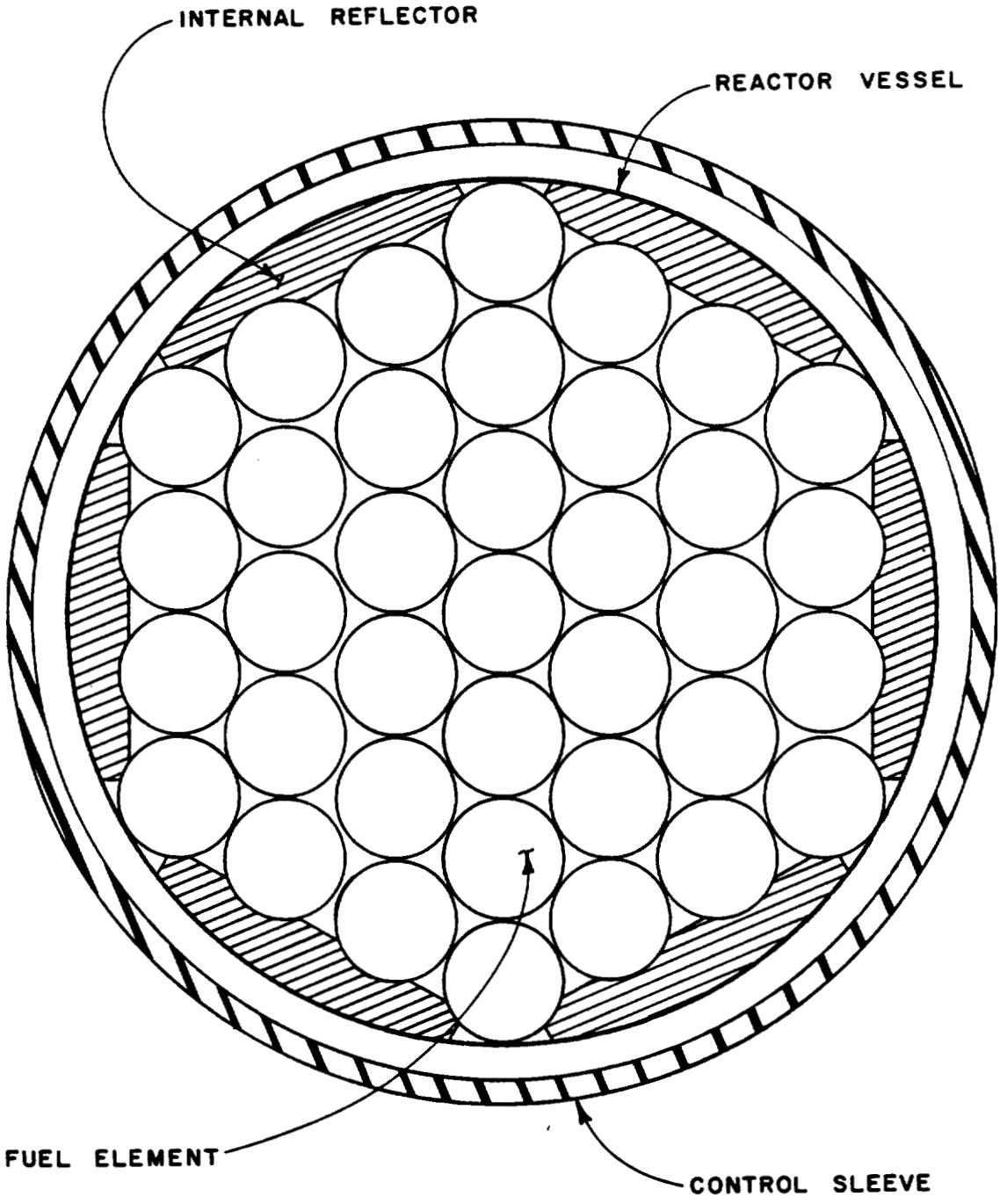

Fig. II-3 SNAPTRAN-3 Reactor Cross Section.

1256005

III. OPERATION SUMMARY

1. Static Physics Measurements

Prior to the destructive test the reactor's static characteristics were investigated by determining the poison sleeve and critical water height configurations. The excess reactivity was also determined from a normalized sleeve-worth curve and found to be 3.80 ± 0.20 dollars.

2. Power Calibration

Also prior to the destructive test the core was operated at 2.0 kw for approximately 2 hours. Details of both the power calibration and the static physics measurements are presented in IDO-17019, "SNAPTRAN 2/10A-3 Destructive Test Results"[1].

Although these runs were of quite short duration, the total integrated energy release was calculated to be 11.7 Mw-sec with a corresponding contribution to the fission product inventory of the core at the time of the destructive test 49 days later. A calculation of the anticipated total fission product inventory of the core after the destructive test would therefore require inclusion of the fission products produced by the power calibration. It can be seen that the contribution of a long lived isotope such as Cs-137 would be approximately 20% of the total.

3. Destructive Test

The destructive excursion was intiated by the rapid removal of the poison sleeve from the core by means of an explosive actuator. A brief listing of the nuclear data associated with the destructive test is given in Table I. A more complete discussion and evaluation of the data is reported in IDO-17019, "SNAPTRAN 2/10A-3 Destructive Test Results"[1].

1256006

TABLE I

SNAPTRAN-3 DESTRUCT TEST NUCLEAR DATA

Asymptotic period of the power rise	640 ± 30 μsec
Peak power	18,000 ± 2000 Mw
Total nuclear energy release (most probable)	45 ± 4 Mw-sec
Maximum core averaged fuel temperature	1,900 ± 200°F
Excess reactivity addition	3.75 ± 0.25 dollars
Maximum disassembly pressure	1,000 ± 300 psi

1256007

IV. POST DESTRUCTIVE TEST ANALYSES

1. Core Inspection and Recovery

The test dolly and reactor remains were transferred from the test cell to the TSF area hot shop for the detailed examination of the fuel and components a week after the destructive test.

The first phase of the fuel recovery operation included removal of the superstructure which supported the poison sleeve drive mechanism and the Edgerton, Germeshausen and Grier periscopes. This was accomplished by remote methods with the hot shop manipulators.

1.1 Core Distribution

Removal of the superstructure and periscopes allowed direct manipulator access into the environmental tank for recovery of the reactor fuel and components. Figure IV-1 shows the distribution of the fuel over the bottom of the environmental tank as a result of the destructive excursion. Although the distribution appears random, the reactor fuel and components were in fact recovered from areas of the environmental tank floor corresponding approximately with their original locations in the assembled core before the destructive disassembly. This indicates that the disassembly was generally symetrical from the center of the core outwards as was shown by the Edgerton, Germeshausen and Grier core profile pictures[1] and is also indicated in Figure IV-2 of the six beryllium reflector pieces which were broken essentially in the center in all cases.

1.2 Fuel Recovery and Size Distribution

All fuel pieces and cladding of sufficient size were removed from the environmental tank by remote manipulators and examined for identifying marks. Figure IV-3 shows the identified fuel and cladding arranged in the pre-test core configuration. Approximately 50% of the original core weight in fuel and cladding was identifiable and 99% of the core recovered. The remaining 1% is presumed to have been either flushed out with the environmental tank water to the waste tank and/or

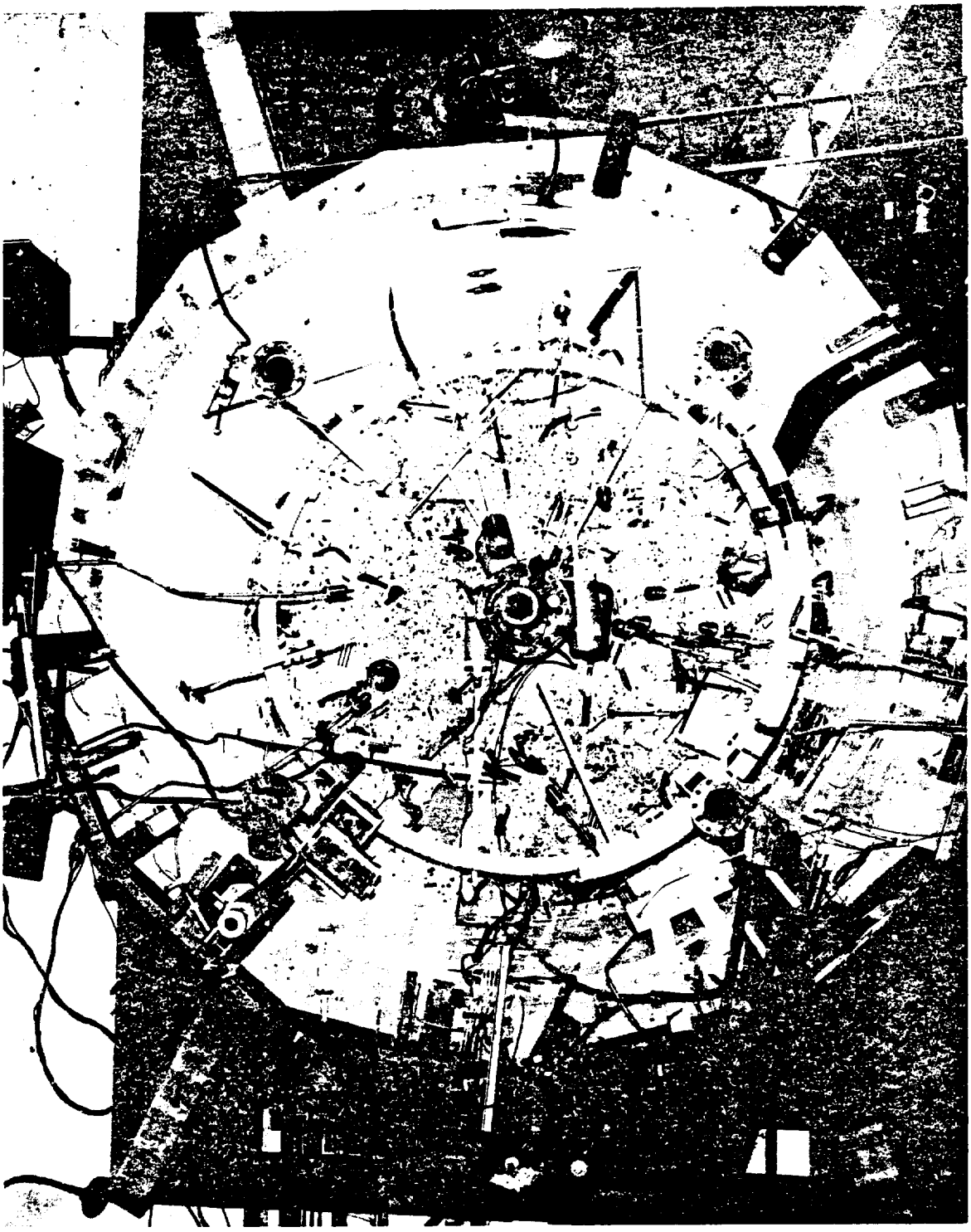

Fig. IV-1 Post-Test Remains of Reactor after Removal of Superstructure.

1256009

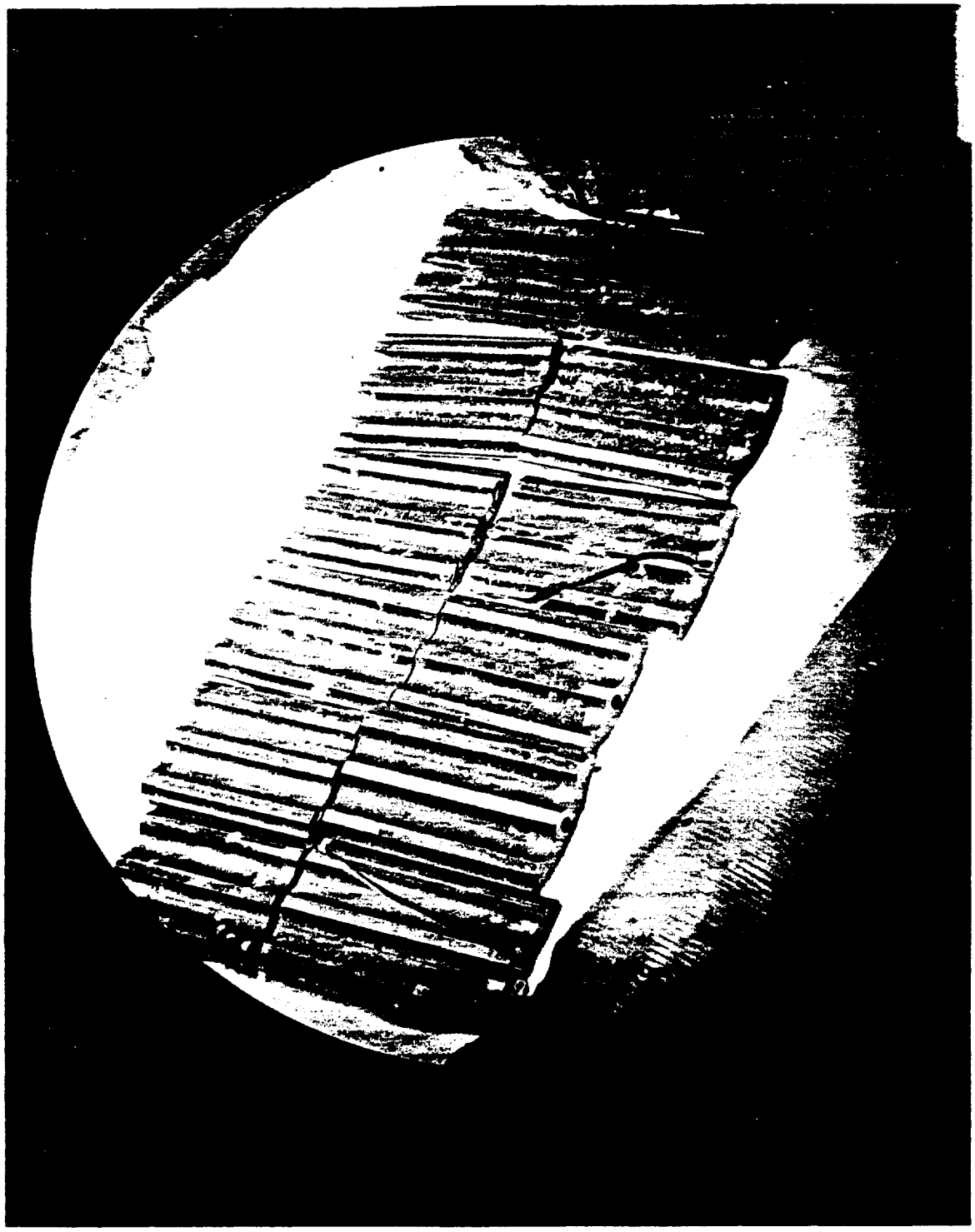

Fig. IV-2 Beryllium Reflectors after Destructive Test.

1256010

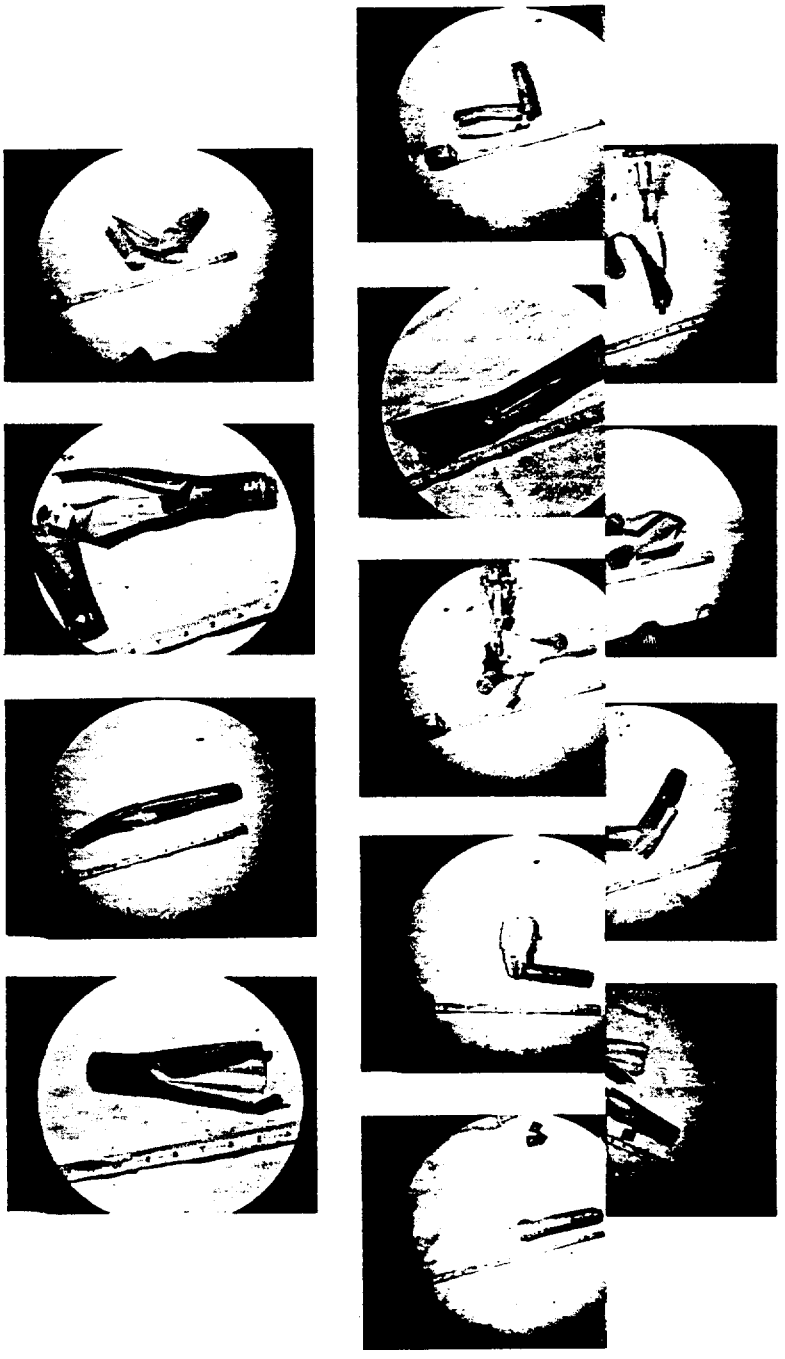

Fig. IV-3 Fuel Rod Remains Arranged

1256011

Fig. IV-4 Small Fuel Pieces Recovered by Vacuum Cleaning.

blown out of the environmental tank onto the test pad and surrounding ground during the test. Although no fuel pieces were recovered outside of the environmental tank in the test cell area, the general area contamination was 500-800 dpm 24 hours after the test.

Fuel pieces that were too small to be recovered efficiently by manipulator were picked up by vacuum cleaner. The total amount recovered by this method was approximately one third of the core. Figure IV-4 shows a typical tray of material recovered by vacuum cleaning from the environmental tank floor. The distribution of this fine material is given in Table II.

TABLE II

SIZE ANALYSIS OF FINES

Tyler Screen Size	wt. gms.	wt.%
> 4	11,930	75.5
> 16	2,776	17.6
> 100	1,016	6.3
> 200	75	0.5
< 200	13	0.1
Total	15,810 gms	100%

A sample of the < 200 mesh size fines was examined by microscope to determine the distribution of the particles as to size and type of material. The results are presented in Table III. The green and white materials in the table are probably hydrogen barrier present in two different states resulting from different peak temperatures in the fuel.

Some of the white material may be zirconium oxide. The three metal types are presumed to be uranium and zirconium compounds. The sources of the small amount of red material and iron have not been identified but presumably did not originate in the core. The quartz and glass undoubtedly were from the Edgerton, Germeshausen and Grier photographic "backup" lights which were shattered by the shock wave from the core disassembly.

TABLE III

PARTICLE DISTRIBUTION, < 200 MESH

Type of Material	Percent of sample	Size in Microns (Expressed at % of Type) 0-10	10-20	20-30	30-40	40-50	50-60	60-80	80-120	120-200
Green Chunks	20	< 1	5	5	5	10	20	40	10	5
White Balls	< 1	[illegible]		5	20	20	20		5	
White Chunks	1	< 1		10	10	10	10	50	5	5
Metal Shavings	5	< 1						20	30	50
Metal Balls	10	< 1	15	20	20	30	10		5	
Metal Chunks	40	< 1	5	10	10	15	20	20	10	10

1256013

TABLE III (Cont.)

PARTICLE DISTRIBUTION, < 200 MESH

Type of Material	Percent of sample	Size in Microns (Expressed at % of Type) 0-10	10-20	20-30	30-40	40-50	50-60	60-80	80-120	120-200
Red Chunks	< 1	< 1			15	50	30	5		
Quartz	20	< 1		10	10	10	20	30	15	5
Glass	< 1	< 1				90			10	
Iron	3	< 1				50	30	10	5	5
Percent	100%		2.5	6.0	9.0	31.5	16.0	17.5	17.5	8.0

1.3 Core Sampling

Several representative fuel pieces were sampled for both chemical and metallurgical analysis. Figure IV-5 is the original core layout including both the core location number (above) and the fuel element number below (i.e., E-65). Sample wafers were cut from elements E-65, E-151, E-153, and the bottom of E-84. The wafers from E-65, E-151, and E-153, for chemical analysis, were cut from each end of each fuel element as well as from either side of the missing center sections, resulting in four wafers from each fuel element. The wafers were numbered 1 through 4 starting at the bottom of each element and were identified as 65-1, 65-2, 65-3, etc. Their location on the original fuel element and approximate thickness are given in Table IV. Additional samples were also taken from E-65, E-151, E-153, and the bottom of E-84 for metallurgical analysis.

TABLE IV

SAMPLE WAFER IDENTIFICATION AND LOCATION

Sample Identification	Original Location	Approximate Thickness
65-1	12-1/4 - 12-1/2 from top shoulder	1/4"
65-2	8 - 8-1/2 from top shoulder	1/2"
65-3	3-1/2 - 4 from top shoulder	1/4"
65-4	0 - 1/4 from top shoulder	1/4"

1256014

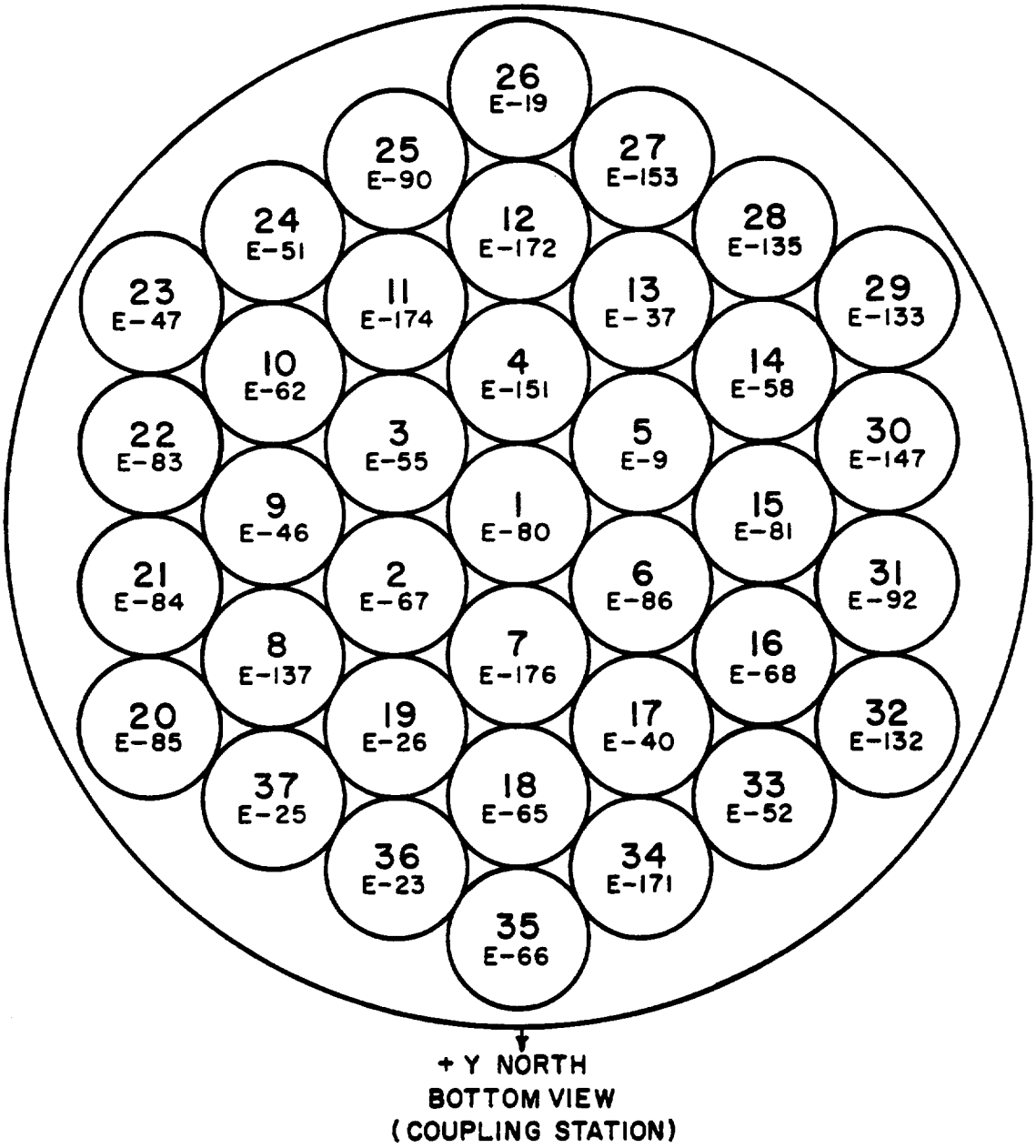

Fig. IV-5 SNAPTRAN-3 Core Layout.

1256015

TABLE IV (Cont.)

SAMPLE WAFER IDENTIFICATION AND LOCATION

Sample Identification	Original Location	Approximate Thickness
151-1	12-1/8 - 12-1/2 from top shoulder	3/8"
151-2	10-3/8 - 10-3/4 from top shoulder	3/8"
151-3	2-1/8 - 2-1/2 from top shoulder	3/8"
151-4	0 - 3/8 from top shoulder	3/8"
153-1	12-3/8 - 12-1/2 from top shoulder	1/8"
153-2	9-1/4 - 9-5/8 from top shoulder	3/8"
153-3	2 - 2-3/8 from top shoulder	3/8"
153-4	0 - 1/8 from top shoulder	1/8"

Note: The cladding was removed from all the sample wafers immediately following cutting except 65-3 and 151-3. These two cladding rings were used for Cr^{51} activation analysis and are discussed elsewhere in this section. Also, the sections of the original fuel elements between the -2 and -3 wafers were missing following the destructive test.

2. Chemical Analysis

2.1 Hydrogen Distribution

The hydrogen analysis of the fuel by vacuum extraction was intended to indicate the amount of hydrogen released from various areas of the core during the destructive test. Radial and longitudinal hydrogen distribution was determined in the wafers cut from E-65, E-151, and E-153 (Table IV) and spot determinations made on the top section of E-147, the spongy appearing fuel of the bottom section of E-84, and samples of the following fine materials: -16 + 100 mesh, -100 + 200 mesh, and < 200 mesh. The resulting values have a 95% confidence interval of $\pm$ 0.02 wt%.

The wafers listed in Table IV were sampled radially by taking five samples from each wafer from the center outward. The samples were identified by H-1 at the center to H-5 at the edge and the results of the hydrogen analyses given in Table V.

The spot hydrogen analyses of the remaining fuel pieces and fines are presented in Table VI. The percentage of the original hydrogen that was apparently released by the destructive test from all the fuel pieces analyzed is also given in this table for comparison. The sampling positions on E-147 and E-84 correspond approximately with wafer positions -4 and -2 respectively on fuel elements E-65, E-151, and E-153. It was also assumed that the original H_2 content of the fine material was 1.80 wt.% in calculating the percentage hydrogen loss in the table.

The results of the hydrogen loss indicate that there was essentially no loss of hydrogen from the extreme ends of the fuel elements and only a 10-15% loss at the broken ends of elements E-65 and E-151. Element E-153 located at the outside edge of the core apparently had a negligible hydrogen loss even at the broken ends. A close examination of the hydrogen content of the five samples from each of the -2 and -3 wafers indicates that the surface appearance (cracks and fissures) probably explains the wide range of results reported. In several cases the edges of the cracks were a much darker color than the remainder of the wafer indicating an oxide formation or a change in structure resulting in variable hydrogen loss. Figure IV-6 is an example of crack formation in E-65-3. The hydrogen losses from E-147 (147-4) and E-84 (84-2) compares reasonably well with the loss from the corresponding locations in E-65 and E-151. The slightly higher loss from E-84 may be explained by the spongy appearance that is very similar to the darker colored edges of the cracks in Figure IV-6. The hydrogen loss from the fine fuel material indicates that the finer the material, the greater the hydrogen loss. It may be deduced that the fuel in the higher flux areas of the core received the greatest physical damage and a correspondingly greater hydrogen release from the fuel matrix.

1256017

TABLE V

HYDROGEN ANALYSIS

E-65 Original H_2 1.80 wt%	Sample Appearance	E-151 Original H_2 1.81 wt%	Sample Appearance	E-153 Original H_2 1.78 wt%	Sample Appearance
65-1		151-1		153-1	
H-1 1.79 wt%	No cracks in fuel	H-1 1.73 wt%	No cracks	H-1 1.69 wt%	No visible cracks
H-2 1.78		H-2 1.75		H-2 1.72	
H-3 1.84		H-3 1.74		H-3 1.73	
H-4 1.77		H-4 1.73		H-4 1.73	
H-5 1.84		H-5 1.76		H-5 1.71	
avg 1.80		avg 1.74		avg 1.72	
65-2	Large cracks many fissures	151-2	Pitted, numerous cracks	153-2	Cracks and fissures darkened at edge
H-1 1.43 wt%		H-1 1.67 wt%		H-1 1.71 wt%	
H-2 1.52		H-2 1.55		H-2 1.71	
H-3 1.39		H-3 1.50		H-3 1.63	
H-4 1.53		H-4 1.72		H-4 1.72	
H-5 1.74		H-5 1.73		H-5 1.70	
avg 1.52		avg 1.63		avg 1.69	
65-3		151-3		153-3	
H-1 1.55 wt%	Numerous cracks and fissures	H-1 1.44 wt%	Pitted, numerous cracks	H-1 1.72 wt%	Pitted, numerous cracks
H-2 1.38		H-2 1.43		H-2-1.72	
H-3 1.50		H-3 1.58		H-3 1.73	
H-4 1.47		H-4 1.56		H-4 1.72	
H-5 1.69		H-5 1.57		H-5 1.67	
avg 1.52		avg 1.52		avg 1.71	
65-4		151-4		153-4	
H-1 1.77 wt%	No cracks in fuel	H-1 1.75 wt%	No visible cracks	H-1 1.73 wt%	No visible cracks
H-2 1.77		H-2 1.74		H-2 1.70	
H-3 1.80		H-3 1.77		H-3 1.71	
H-4 1.80		H-4 1.74		H-4 1.71	
H-5 1.85		H-5 1.73		H-5 1.73	
avg 1.80		avg 1.75		avg 1.72	

1259018

Fig. IV-6 Cross Section 4-1/2 inches from the Bottom of Fuel Element E-65 (E-65-3).

1256019

TABLE VI

SPOT HYDROGEN ANALYSES AND PERCENTAGE HYDROGEN LOSS

Sample	
Top E-47 (orig. H_2 1.78 wt.%)	1.63 wt.%
Bottom (spongy) E-84 (orig. H_2 1.775 wt.%)	1.40 wt.%
-16 + 100 mesh	1.10 wt.%
-100 + 200 mesh	.493 wt.%
< 200 mesh	.399 wt.%

Sample	Avg. Loss	Sample	Avg. Loss	Sample	Avg. Loss	Sample	Avg. Loss
65-1	0%	151-1	4%	153-1	3%	147-4	8%
65-2	16%	151-2	10%	153-2	5%	84-2	20%
65-3	16%	151-3	16%	153-3	4%	-16 + 100	39%
65-4	0%	151-4	3%	153-4	3%	-100 + 200	73%
						< 200	78%

2.2 Fission Product Distribution

The remaining portion of each fuel wafer and the sieved fine fuel were analyzed for the following fission products: I-131, Ba-140, Ce-141, Zr- 95, Cs-137, Sr-89-90 and Ru-103 and are presented in Table VII. The results give a longitudinal but not a radial distribution of the fission products for the three fuel elements and indicate that the flux was higher near the center of each fuel element than at the ends. The variations in the I-131 results for the fuel elements may be attributed to sublimation and/or migration of the iodine. Although the strontium analysis was made for both the Sr-89 and Sr-90 isotopes, the disintegrations from the Sr-89 represents > 99% of the total strontium activity. Consequently, the Sr-90 was not detectable.

1256020

TABLE VII

FISSION PRODUCT DISTRIBUTION

(Expressed as μc/gm at T + 2.28 hrs.)

Sample No.	I^{131}	Ba^{140}	Ce^{141}	Zr^{95}	Cs^{137}	Sr^{89}	Ru^{103}
65-1	16	24	1.7	2.2	.026	4.7	.21
65-2	23	47	3.0	4.6	.049	8.8	.51
65-3	8	44	3.1	4.6	.057	8.4	.23
65-4	23	23	1.3	2.1	.029	3.5	.28
151-1	10	25	1.3	2.4	.025	4.6	.27
151-2	22	39	1.8	3.9	.046	7.3	.30
151-3	27	46	2.3	4.6	.057	8.1	.50
151-4	15	23	1.2	2.2	.028	4.5	.26
153-1	15	21	1.1	2.1	.024	3.8	.24
153-2	17	34	1.7	3.4	.036	5.8	.35
153-3	12	34	2.0	4.0	.026	6.6	.31
153-4	----------	----------	Lost Sample	----------	----------	----------	----------
-16 + 100 mesh	5.62×10^{1}	19.5	3.0	.97	.41	14.9	12.5
-100 + 200 mesh	none detected	6.3	1.8	3.1	1.54	4.5	7.0
< 200 mesh	none detected	31.7	4.6	6.7	1.27	22.9	10.6

	wt.% U	U-235
-16 + 100 mesh	6.71	92.94
-100 + 200 mesh	4.16	92.66
<200 mesh	5.69	92.29

1256021

The analyses of the sieved fine fuel, also presented in Table VII, were corrected for foreign material in the samples (Table III) by assuming no burnup and adjusting the quantity of each isotope reported on the basis of 10.0 wt.% uranium.

The inconsistency of the fines analyses, despite the adjustment, can only be attributed to the presence of variable quantities of foreign materials which would react with the analytical reagents and produce erroneous results. The visual analysis of the < 200 mesh sample presented in Table III indicates that approximately 55% may be fuel and 45% foreign material. This checks quite well with the total uranium in Table VII of 56.9% of the anticipated 10.0% uranium in the fuel.

2.3 Activation Analysis

Several components of the reactor core and vessel were radioautograph and also analyzed by standard activation analysis techniques to determine the flux profile both radially and longitudinally by the two methods. Included in this study were the upper and lower grid plates, a longitudinal strip of the reactor vessel, and a longitudinal strip of fuel element E-86 cladding.

The components included in the activation analysis are shown in Figure IV-7 and the location of samples indicated in Figures IV-8, IV-9, and IV-10. Co-58, by n,p reaction from Ni-58, was used for the activation analysis and was calculated as μc Co-58/gm. total Ni corrected to T_o + 2.28 hours. Results of the analyses are plotted in Figures IV-11 through IV-14, and yield flux shapes, both axially and radially, which were in good agreement with the spatial flux as determined from other means during the destructive test. Activation analysis therefore appears to be a useful post test method for determining the flux shape that existed during a given reactor excursion.

It must be ponted out that the power calibration of the core 49 days prior to the destructive test contributed approximately 14% of the final Co-58 activity in the components corrected to T_o + 2.28 hours. Details of the power calibration are covered in IDO-17019, "SNAPTRAN 2/10A-3 Destructive Tests Results" for calculation of the energy release from the destructive test from the activation results.

1256022

Radioautographs were also made of each of the components included in the activation analysis and densitometer readings taken at the corresponding points of the activation samples for purposes of comparison. The results of the densitometer readings are plotted in Figures IV-15 through IV-18 with the activation results also shown. The radioautographs of the upper and lower grid plates were both taken on the side of the plates towards the reactor core. The upper grid plate was extensively distorted by the destructive test which probably explains the difference between the radioautographs and the activation curves in this case. Intimate film contact with the plate surface was not possible because of the distortion.

The two cladding rings from fuel wafers 65-3 and 151-3, mentioned in the note on Table IV, were analyzed for both total chromium and Cr-51 to determine the extent of chromium activation. The results corrected T_o + 2.28 hrs. are as follows:

Sample Identification	Total Chromium %	Cr-51 μc/gm
63-3	7.36	1.07
151-3	7.36	1.07

The Hastelloy-N cladding for both E-65 and E-151 fuel elements came from the same original tube prior to fabrication and would be expected to have the same total chromium analysis.

3. Metallurgical Examination

3.1 Zirconium Hydride Fuel

Several fuel elements were sampled to determine the core temperature gradients by investigation of phase changes, changes in hardness, and evaluation of crack formation in the zirconium hydride. The locations of the sample points on the fuel elements are shown in Figure IV-19 and also the relative location of the hydrogen-fission product sample wafers described in the previous sub-section. Table VIII lists the fuel element samples and sample mount members.

1256023

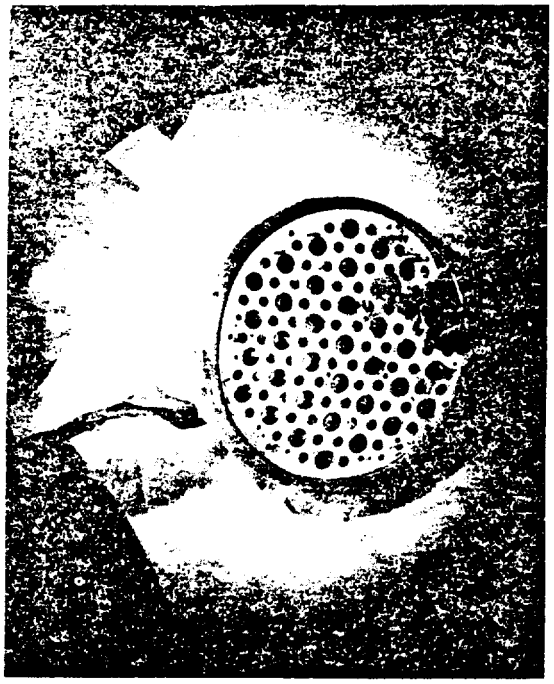

Upper Grid Plate

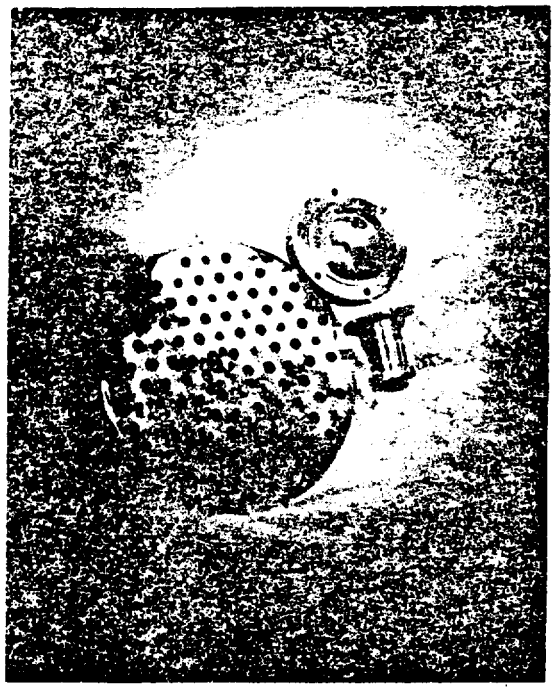

Lower Grid Plate

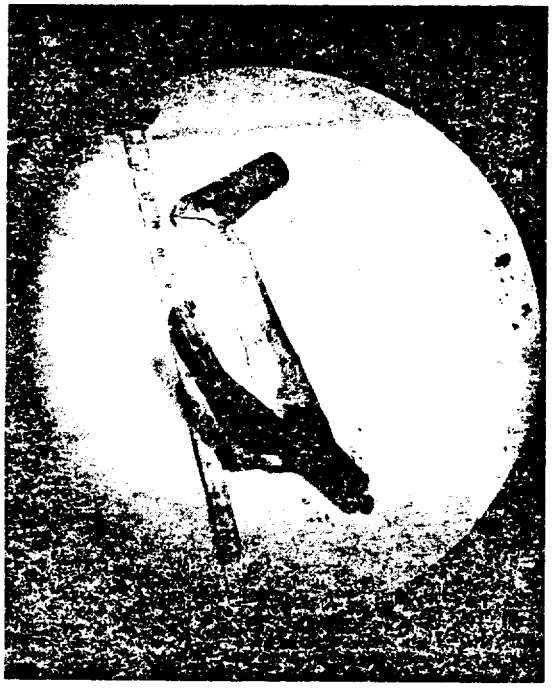

Fuel Element E-86

Reactor Vessel

Fig. IV-7 Components Examined for Activation.

1256024

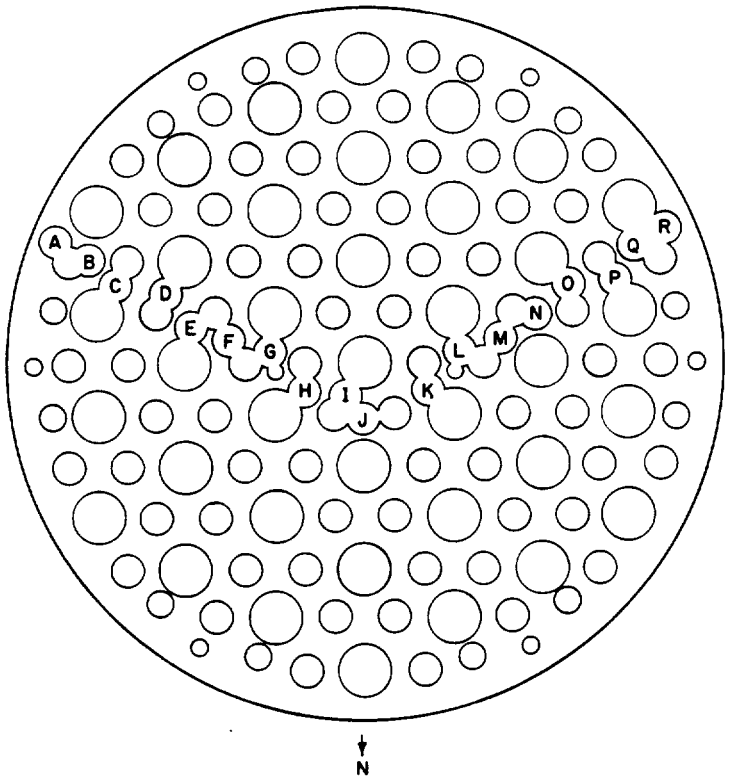

Fig. IV-8 Upper Grid Plate Sample Locations.

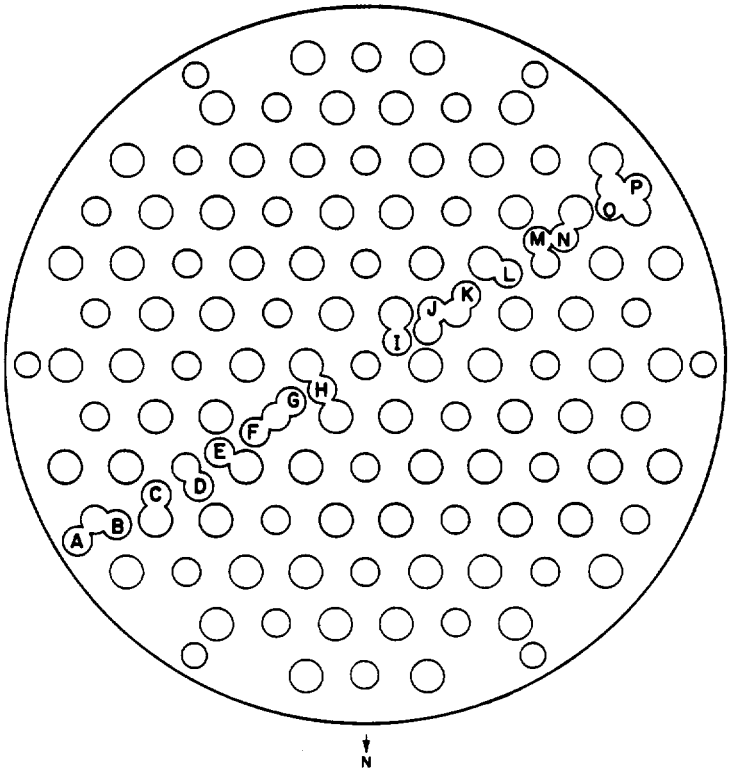

Fig. IV-9 Lower Grid Plate Sample Locations.

1256025

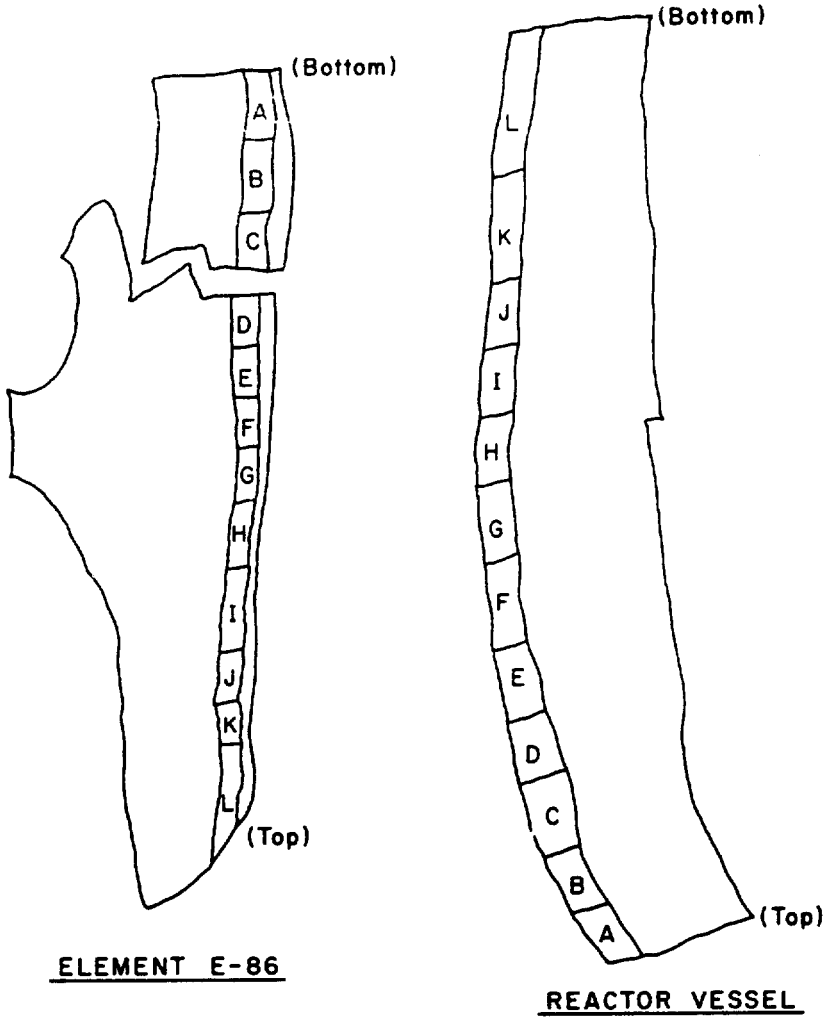

Fig. IV-10 Element E-89 Cladding and Reactor Vessel Sample Locations.

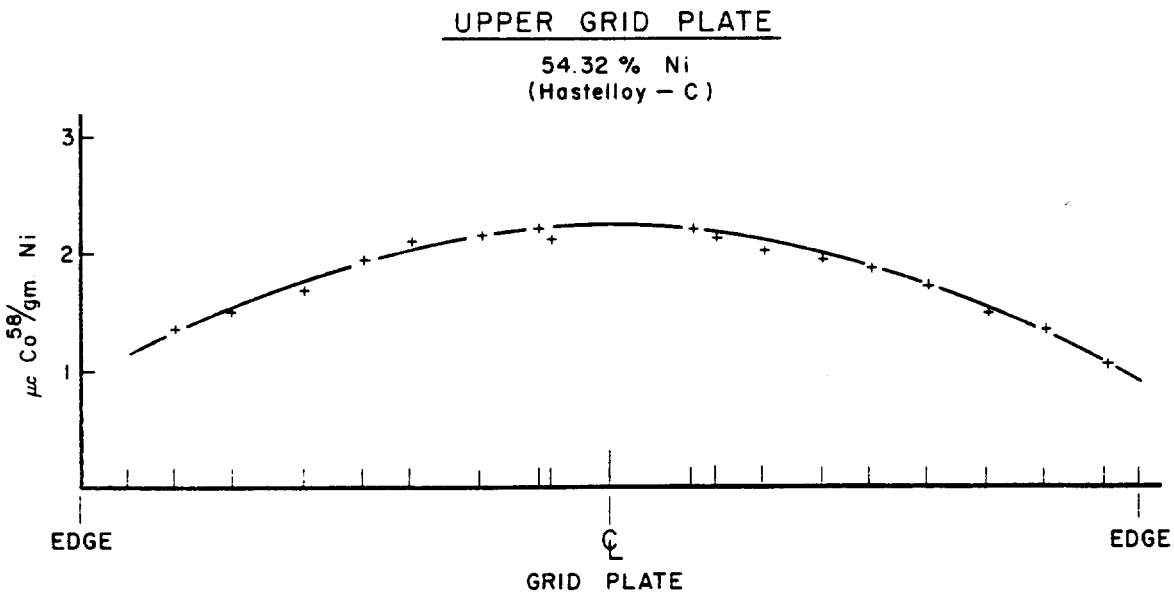

Fig. IV-11 Neutron Activation Across Upper Grid Plate.

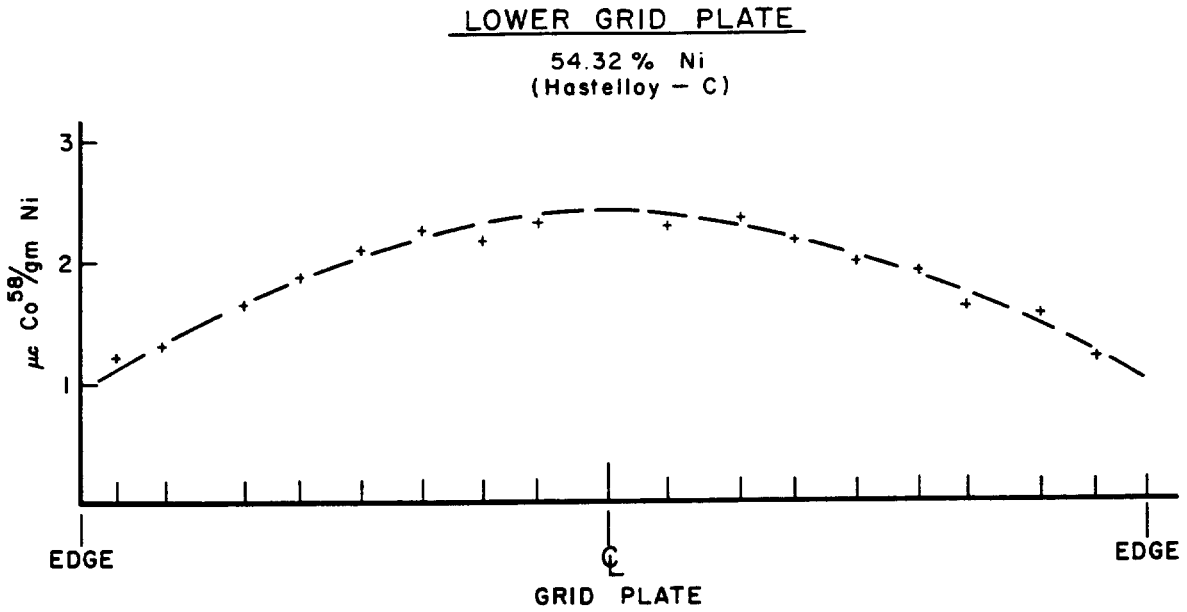

Fig. IV-12 Neutron Activation Across Lower Grid Plate.

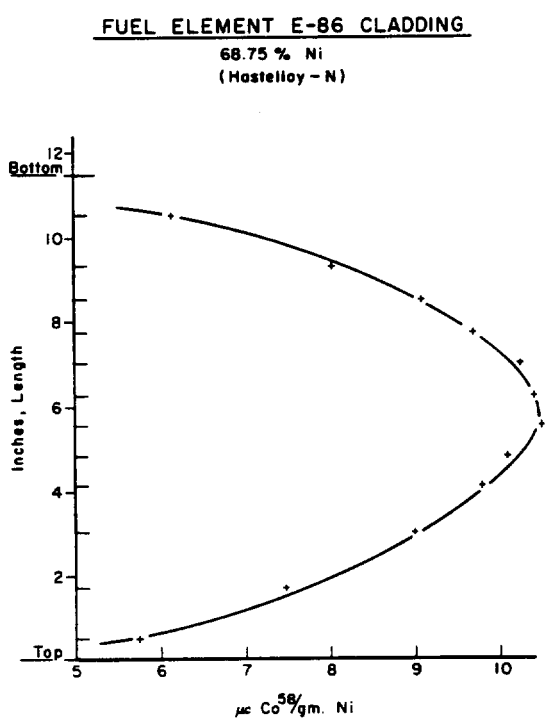

Fig. IV-13 Neutron Activation of Element E-86 Cladding.

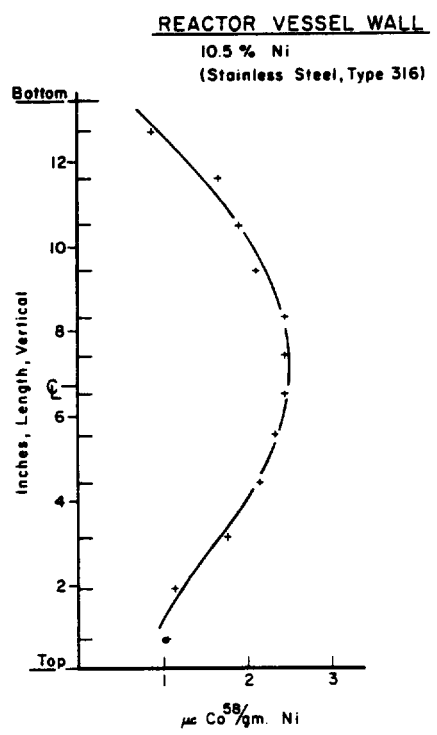

Fig. IV-14 Neutron Activation of Reactor Vessel Wall.

1256027

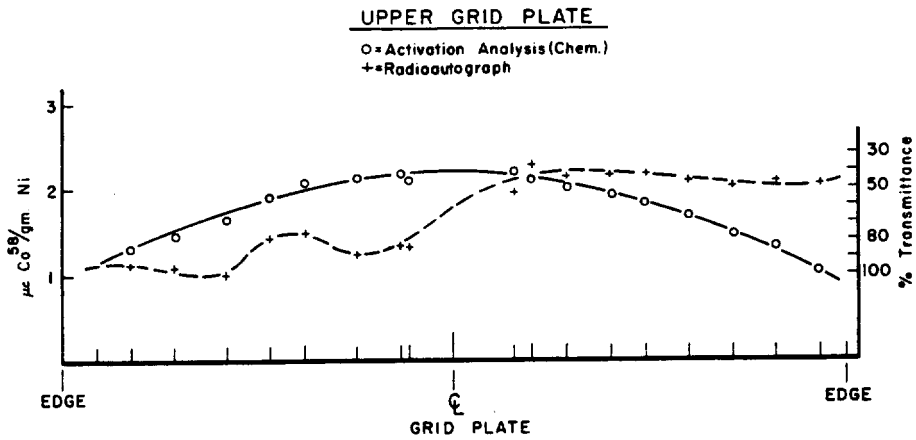

Fig. IV-15 Radioautograph, Upper Grid Plate.

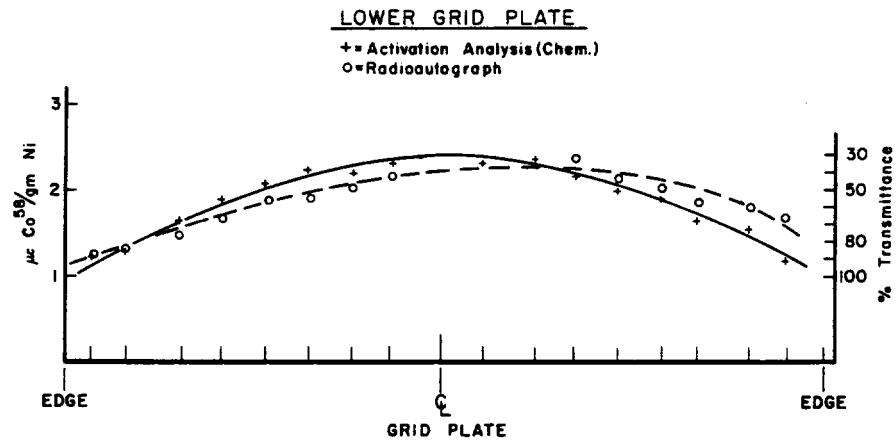

Fig. IV-16 Radioautograph, Lower Grid Plate.

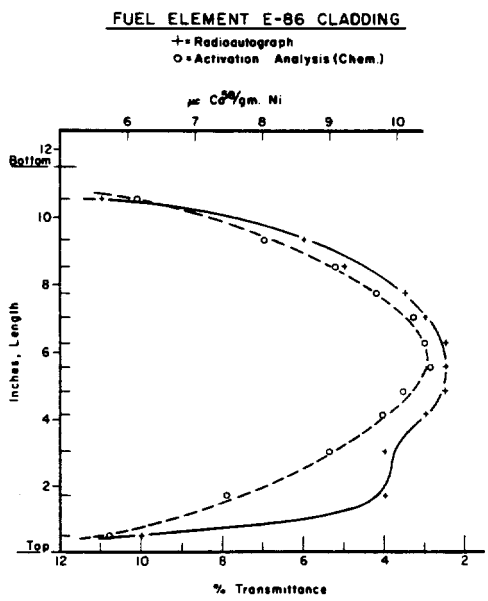

Fig. IV-17 Radioautograph, E-86 Cladding.

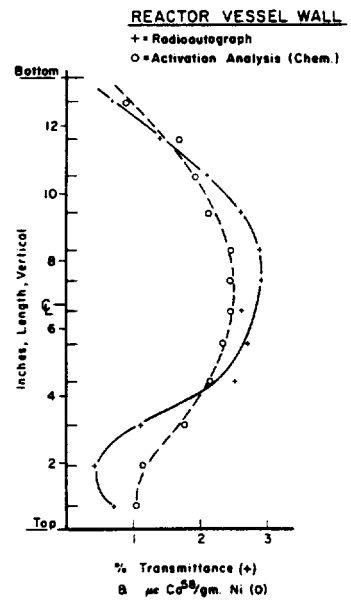

Fig. IV-18 Radioautograph, Reactor Vessel Wall.

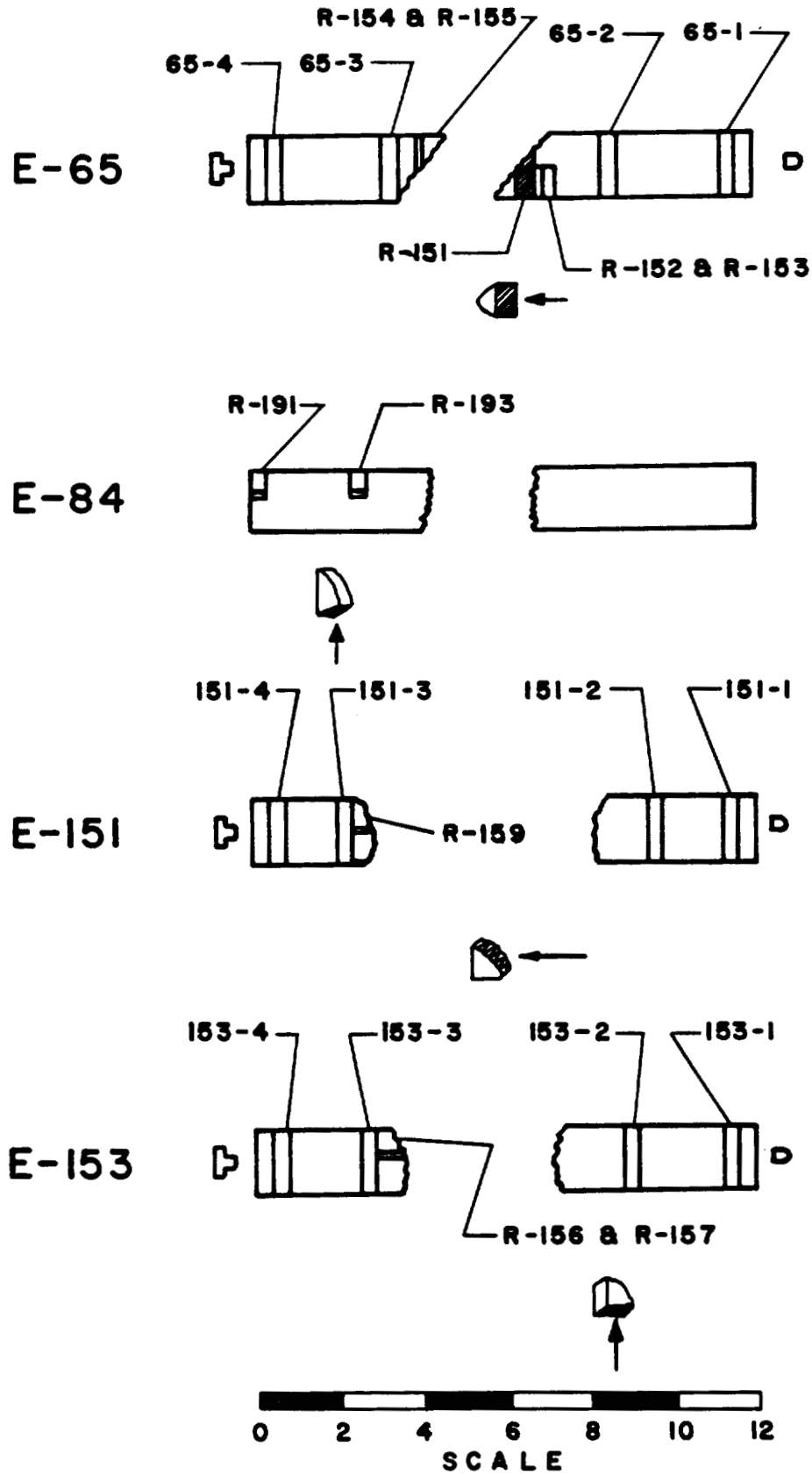

Fig. IV-19 Fuel Element Sample Locations.

1256029

TABLE VIII

METALLOGRAPHY SAMPLES

Fuel Element	Mount No.	Description
E-65	R-151	Fuel, sample taken 5" from bottom of pin.
	R-152	Fuel, sample taken 4-1/2" from bottom of pin.
	R-153	Fuel, sample taken 4-1/2" from bottom of pin, numerous cracks.
	R-154	Fuel, sample taken 3-1/2" from top of pin, transverse plane of fissured section.
	R-155	Fuel, sample taken 3-1/2" from top of pin, adjacent to piece R-154.
	R-160	Clad, sample 4-1/2" to 5-1/2" from bottom of pin, flat section with rupture termination.
	R-161	Clad, sample 4-1/2" to 5" from top of pin, transverse section, contains longitudinal tear.
	R-162	Clad, sample 5" from bottom of pin, longitudinal section, contains transverse tear.
	A-165	Cladding, three specimens A, B, and C. Transverse section, button end half of element.
	A-166	Cladding, specimen mounted flat, contains termination of longitudinal tear, button end.
E-84	R-163	Clad, sample 6" from top of pin, longitudinal section, contains transverse tear.
	R-164	Clad, sample 7" from bottom of pin, longitudinal section, contains transverse tear.
	R-191	Fuel, one quarter wafer section mounted longitudinally taken from cold end of pin.
	R-193	Fuel, one quarter wafer section mounted longitudinally taken 2-1/2" from cold end of fuel pin.
	A-173	Cladding, three specimens A, B, and C. Transverse sections, tears next to negator, button end half of element.

1256030

TABLE VIII (Cont.)

METALLOGRAPHY SAMPLES

Fuel Element	Mount No.	Description
E-84	A-174	Cladding, specimen mounted flat, contains termination of longitudinal tear, button end.
	A-175	Cladding, specimen mounted in the transverse section, full circumference of cladding near end of element (button end).
E-151	R-158	Clad, sample taken 3" from top of pin, flat section with rupture termination.
	R-159	Fuel, sample 2-3/8 to 3" from top of pin, cross section of pin.
E-153	R-156	Fuel, sample taken from 3" from top of pin, cross section of pin.
	R-157	Fuel, sample taken 3" from top of pin, adjacent to R-156.
	R-165	Fuel, sample (unidentified), longitudinal section.
	R-166	Fuel, sample (unidentified), transverse section.
Reactor Vessel	R-178	Transverse section, wall, held in negator with torn edge of wall away from the negator, the torn edge representing the rupture break of the vessel.
Reactor Vessel	R-179	Cladding, longitudinal section of reactor vessel wall mounted flat, the notched end is the torn edge of the break.
Unidentified	R-192	Fuel, unidentified, blown free of element during test.

3.11 Phase Relationships

The interpretation of changes in microstructure in the samples is based on the presence and/or absence of the following described constituents:

(1) Fuel - small black particles.

(2) Banding - the presence or absence of the banded structure within grain.

(3) Grain size - delineated by grain boundries or by boundries as defined by banding orientations.

(4) Cracking - observed as both microcracks and large cracks.

(5) Voids - black areas slightly larger than the fuel particles or as the dark areas at the edge of islands.

(6) Additional phases - (a) elongated light particles forming along cracks.

(b) heavier appearing parallel structures forming along cracks.

(c) a brown structur forming both along the edge of the cracks and also slightly in the internal portion of the matrix at the cracks.

(d) dark particles in the matrix larger than fuel particles

Three fuel samples, R-191, R-192, and R-193 were chosen as typical microstructures encountered in the investigation. The three specimens consisted of a sample of the intact fuel at the "cold" end of a fuel element (R-191 from element E-84), a sample from the "midpoint" of the intact fuel (R-193 from element E-84), and a "hot" sample of fuel which had been completely severed from an element (R-192 from an unidentified fuel element).

Three distinct phases appear to be predominant in the three samples. They are epsilon zirconium-hydride, delta zirconium-hydride, and gamma zirconium-hydride. The epsilon phase appears to be the only zirconium-hydride phase present in the cool portions of the element. This is the banded equiaxed grains shown in Figure IV-20 from R-191. In the next "hotter" portion of the element (R-193) both the epsilon (banded equiaxed structure) and delta (unbanded equiaxed grain structure) phases are present as shown in Figure IV-21 and a small amount of the gamma phase

1256032

(small white elongated particles in Figure IV-22). The same appearance description of the delta phase had been previously reported in the literature by Beck[2], Shoop[3], and Filer, et al[4]. In the hottest region of an element (R-A2), there appears only the delta phase (Figure IV-23) and an increase in the amount of gamma phase (parallel appearing structure along crack in Figure IV-24).

The transformation of epsilon to delta zirconium-hydride appears to be promoted by a decrease in hydrogen content according to phase diagrams by Beck[2] and Vetrano and Atkins[5]. There also appears to be evidence that the retention of epsilon plus delta structures (R-193) is dependent upon temperature and associated cooling rates since these two phases are present in unfractured portions of the fuel in apparently random crystallographic orientations. The epsilon to delta transformation (R-191 to R-192) has been attributed to a diffusionless mechanism in a shear or twinning process by Beck[2] and Vetrano and Atkins[5] and therefore may be extremely sensitive to hydrogen content, temperature, or cooling rate. This phase change, if it is due to loss of hydrogen, may be caused by disassociation of zirconium-hydride at temperature above 700°C (1290°F) (this is an effective minimum temperature proposed by the various structure changes) according to Vetrano and Atkins[5]. This temperature appears realistic when it is noted that aging epsilon zirconium-hydride at 600°C (1100°F) for 500 hours by Beck[2] did not produce any phase change which could be detected metallographically or by x-ray diffraction analysis. The formation of the gamma phase has been proposed by Beck[2] to be a diffusion controlled twinning process from the delta phase. The appearance of the proposed gamma phase in the SNAPTRAN fuel (Figure IV-24) resembles a structure which is developed along crystallographic planes as would a twinned structure. The formation of the gamma phase in the fuel occurs only along cracks as pointed out previously in Figure IV-24 and is also shown in Figure IV-25 which was sample R-151 cut from element E-65. The fact that this phase is apparent only along cracks emphasizes the importance of the loss of hydrogen to the formation of this phase. The average loss of hydrogen from wafer 65-2 was previously

1256033

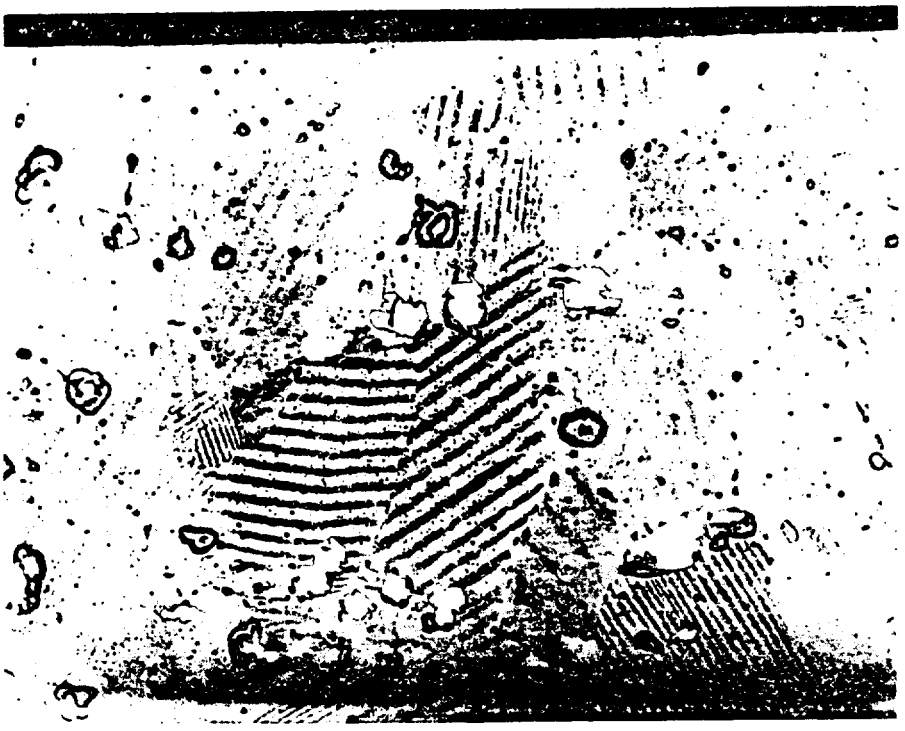

Fig. IV-20 Epsilon Zirconium-Hydrid (Banded Grains), Element E-84, Sample R-191, Stain Etched, 500 x Magnification.

Fig. IV-21 Epsilon (Banded Grains) plus Delta (Unbanded Grains) Zirconium-Hydride, Element E-84, Sample R-193, Stain Etched, 500 x Magnification.

1256034

Fig. IV-22 Gamma Zirconium-Hydride (Elongated White Particles), Element E-84, Sample R-193. Stain Etched, 500 x Magnification.

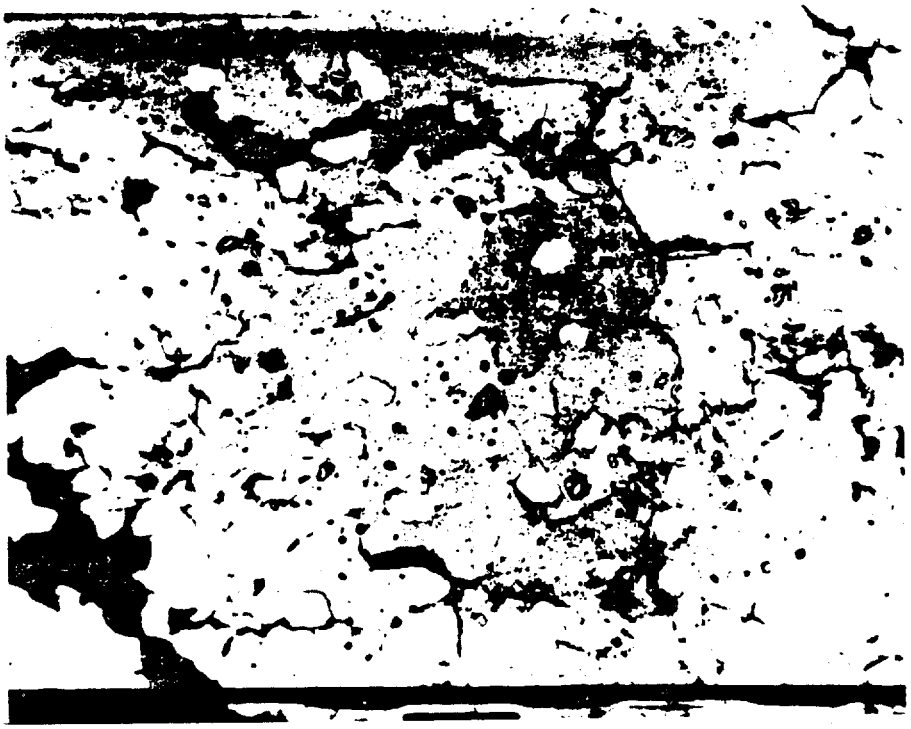

Fig. IV-23 Delta Zirconium-Hydride (Un-Banded Grains), Unidentified Fuell Element, Sample R-192, 500 x Magnification.

1256035

Fig. IV-24 Gamma Zirconium-Hydride (Parallel Appearing Structure Along Crack, Unidentified Fuel Element, Sample R-192, Stain Etched, 500 x Magnification.

Fig. IV-25 Gamma Zirconium-Hydride Formation Along Cracks, Element E-65, Sample R-151, Stain Etched, 500 x Magnification.

1256036

Fig. IV-26 Possible Beta Zirconium-Hydride (Indicated by Arrows) in Matrix of Gamma and Delta Zirconium-Hydride, Unidentified Fuel Element, Sample R-192, Stain Etched, 500 x Magnification.

reported in Section IV-2.1 as approximately 16%. Some possible evidence of the presence of the alpha or beta phase is indicated by the arrows in Figure IV-26. This structure is brownish in color but has not been identified by analysis.

Several metallography samples were further analyzed by x-ray diffraction to more clearly establish the various phases present in the fuel. These samples were chosen on the basis of their typical and representative microstructures and consisted of R-191, R-192, and R-193 (included in the visual phase study), and also R-155 from the "hot" end of element E-65. The x-ray diffraction data is given in Table IX and indicates that R-191 contains only the epsilon zirconium-hydride phase, R-193 contains epsilon, delta, and a small amount of zirconium-hydride, and R-192 and R-151 contain the delta and gamma phases but no epsilon. This data therefore confirms the previous evaluation of the microstructure phases observed.

1256037

TABLE IX

SNAPTRAN 2/10A-3 X-RAY DIFFRACTION DATA /1

dÅ /2 Major Peaks	Phase/3	Relative Intensity (I/Io) Sample R-191	R-193	R-192	R-155
2.81	Alpha			3 /4	
2.75	Epsilon, Delta	100 /5	100 /5	100 /5	100 /5
2.72	Gamma		4	19	10
2.59	Beta		3		
2.56	Alpha-U	11	14	12	15
2.52	Alpha-U	8	9	10	7
2.48	Epsilon, Gamma	21	11	6	5
2.39	Delta		19	45	38
2.29	Epsilon, Alpha-U	4	7	7	5
2.24	Epsilon	20	3		
1.75	Epsilon	9	5		
1.69	Delta, Gamma		24	40	34
1.66	Epsilon	27	13		
1.47	Epsilon	14	7		
1.44	Delta		15	33	23
1.38	Epsilon, Delta, Gamma	13	9	11	17
1.10	Delta		6	11	9

/1 Data obtained by a Norelco X-ray diffraction unit equipped with a goniometer head. The specimens were scanned at a speed of 1 degree (2 theta) per minute using nickel filtered copper K-Alpha radiation.

/2 Only the major peaks are listed in this table.

/3 The phase identifications are according to X-ray diffraction investigations carried out by Beck(2), Filer, et al.(4), and Vaughan and Bridge(6).

/4 The presence of this peak is questionable.

/5 The absolute intensities of these peaks are, in order: 143, 148, 150, and 136.

1256038

The x-ray diffraction data obtained also revealed the presence of the 65.8 atomic percent epsilon phase (reported by Beck[2]) as the major epsilon phase present in R-191 and R-193. Additional "d" values not listed in the table (2.44, 2.29, 1.73) for R-193 indicate the presence of minor amounts of the 62.5 atomic percent epsilon phase as also reported by Beck[2]. Several "d" values, other than the three mentioned above, are not included in Table IX. These "d" values are all of weak intensities and do not match "d" values for the alpha zirconium-hydride phase. One low intensity "d" value found for R-192 (2.59) matches a prominent "d" value of the beta zirconium-hydride phase as reported by Vaughn and Bridge[6] but there were no other values of this phase which appeared in the diffraction data for this sample or any of the other three. If the beta phase is present it may be the brownish structure indicated by the arrows in Figure IV-26.

3.12 Microhardness

A study was made of the relative microhardness of the samples used for the x-ray diffraction phase study (R-191, R-193, R-192, R-155) to determine if a microhardness phase relationship existed. The results, listed in Table X as KHN (Knoop Hardness Numbers), indicate a microhardness range of 132-148 KHN for the epsilon region (R-191), 139-229 KHN for the epsilon-delta region (R-193), and 156-212 KHN for the delta-gamma region. It should be noted that each number in Table X represents an average of five indentations and that all indentations were made in solid fuel although the general area description in some cases consisted of light or heavily cracked. Beck[2] has suggested that the epsilon-zirconium-hydride is softer than the delta phase and shows a hardness range of 220-250 DPH (Diamond Pyramid Hardness) (approximately 235-260 KHN) for the delta region, and 130-250 DPH (approximately 165-260 KHN) for the epsilon region. The broad hardness range of Beck's epsilon plus delta phases is for the respective 65.8 to 62.5 atomic percent (2.08 to 1.81 weight percent) hydrogen composition range. The overall averages for each sample shown in Table X does indicate an increasing hardness from the epsilon (R-191) to the delta-gamma (R-192, R-155) phases.

1256039

TABLE X

FUEL MICROHARDNESS

Sample	Knopp Hardness Number (1 kg. Load)						
	Tested Area						
Fuel	Solid		Light Cracking		Heavy Cracking		Average
R-191	132	148	143	146			142
R-193	139	140	195			229	176
R-192			156	212	193	197	190
R-155			182	192	194	211	195

All hardness numbers listed are an average of five indentations of fuel.

3.13 Cracking

Varying degrees of cracking were observed in essentially all fuel samples. Small intergranular cracks are shown in Figures IV-23, IV-24, and IV-27 and large transgranular noted in Figures IV-22, IV-24 and IV-25. The high temperatures attained during the test are the probable basic causes of this cracking. These temperatures could cause cracking by promoting hydrogen dissociation pressures which would exceed the strength of the zirconium-hydride matrix. The small intergranular cracks may also be the result of thermal expansion and contraction effects caused by high temperature and associated cooling rates. According to Beck[7] the coeficient of thermal expansion of delta zirconium-hydride is approximately 55 percent greater than the epsilon phase. It would therefore be possible for the delta phase, upon forming from the surrounding epsilon phase, to contract more during cooling than the epsilon and cause cracking at the grain boundries. The internal cracking may indicate that the fuel attained temperatures in excess of 950°C (1740°F). This temperature may have been attained or exceeded according to data by Filer, et al.[4] who heat treated zirconium-1.28 hydrogen alloys for 4.5 and 22.5 hours at 950°C and found cracking in the 22.5 hour heat treatment.

1256040

3.14 Uranium Fuel Particles

The uranium fuel appears in the microstructure as the very small black particles in Figures IV-27 and IV-28. No change in particle size, distribution or interaction with the zirconium-hydride matrix could be observed in the samples examined in Figures IV-29, IV-30, IV-31, and IV-32.

1256001

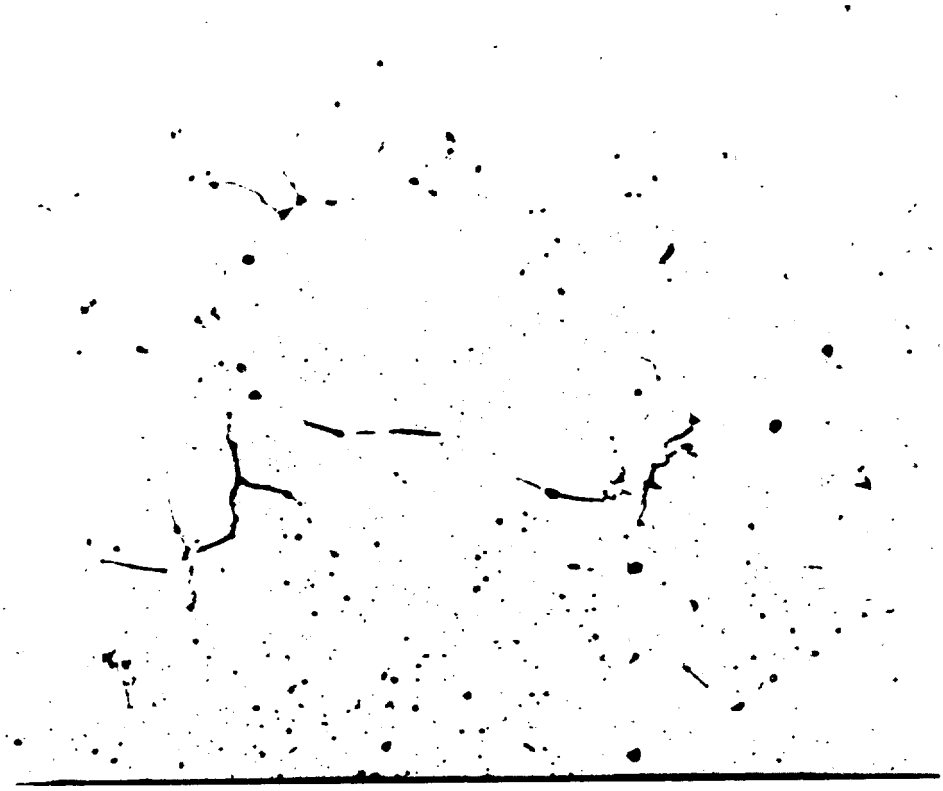

Fig. IV-27 Small Intergranular Cracks, Element E-84 Sample R-193, as Polished, 500 x Magnification.

Fig. IV-28 Small Intergranular Cracks, Unidentified Fuel Element, Sample R-192, as Polished, 500 x Magnification.

1256042

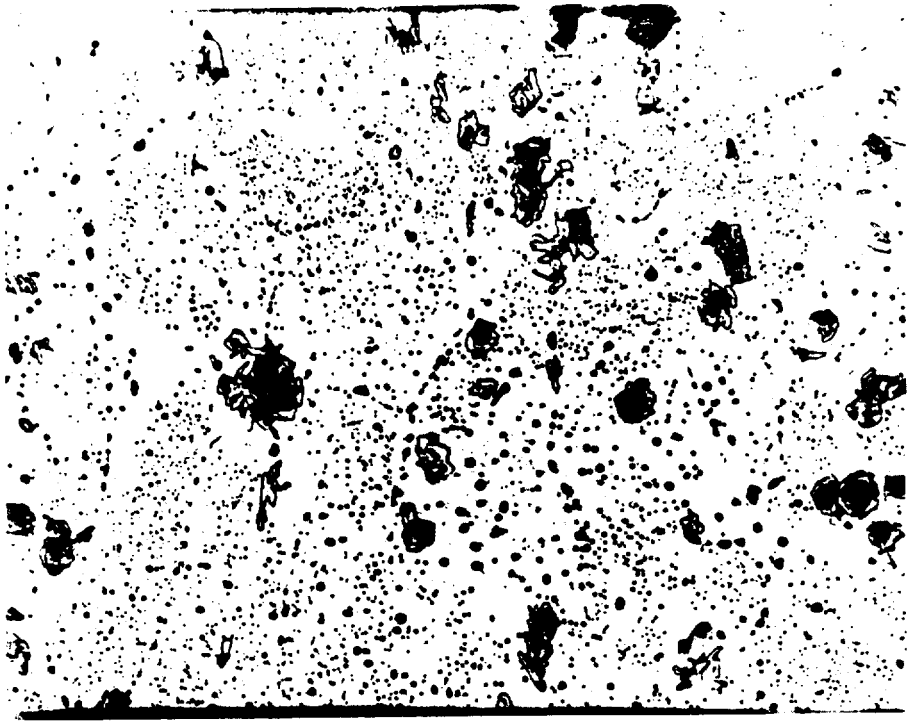

Fig. IV-29 Very Small Fuel Particles and Large Islands with Cored Area, Element E-84, Sample R-191, Etch-Polish-2 for 30 seconds, 500 x Magnification.

Fig. IV-30 Very Small Fuel Particles and Large Islands with Light Coloring, Element E-84, Sample R-193, Etch-Polish-2 for 45 seconds, 500 x Magnification.

1256043

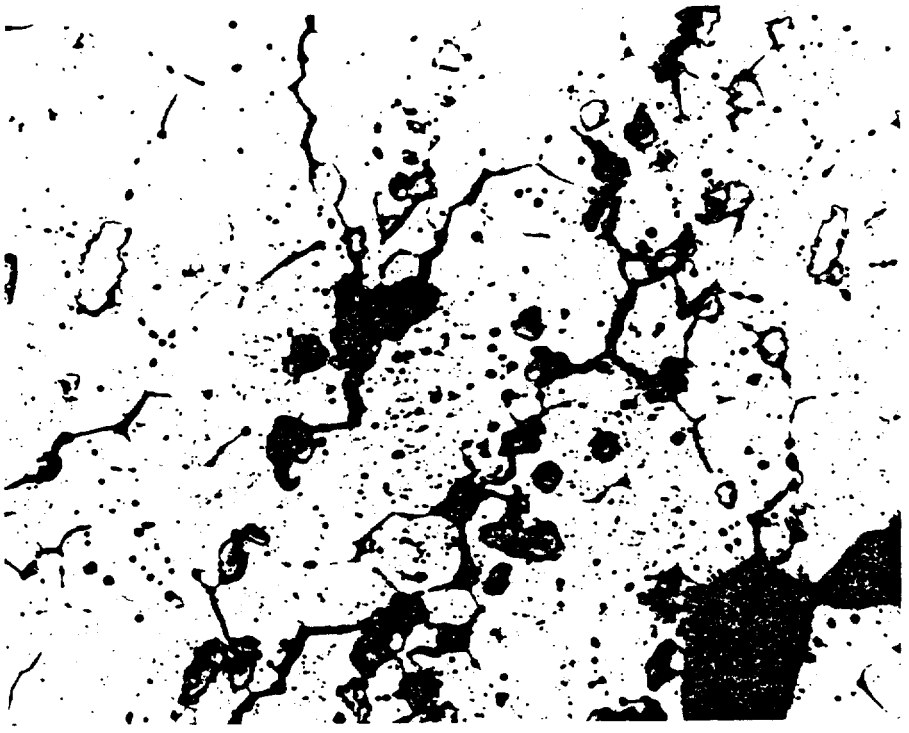

Fig. IV-31 Very Small Fuel Particles and Large Islands with Dark Coloring, Unidentified Fuel Element, Sample R-192, Etch-Polish-2 for 16 seconds, 500 x Magnification.

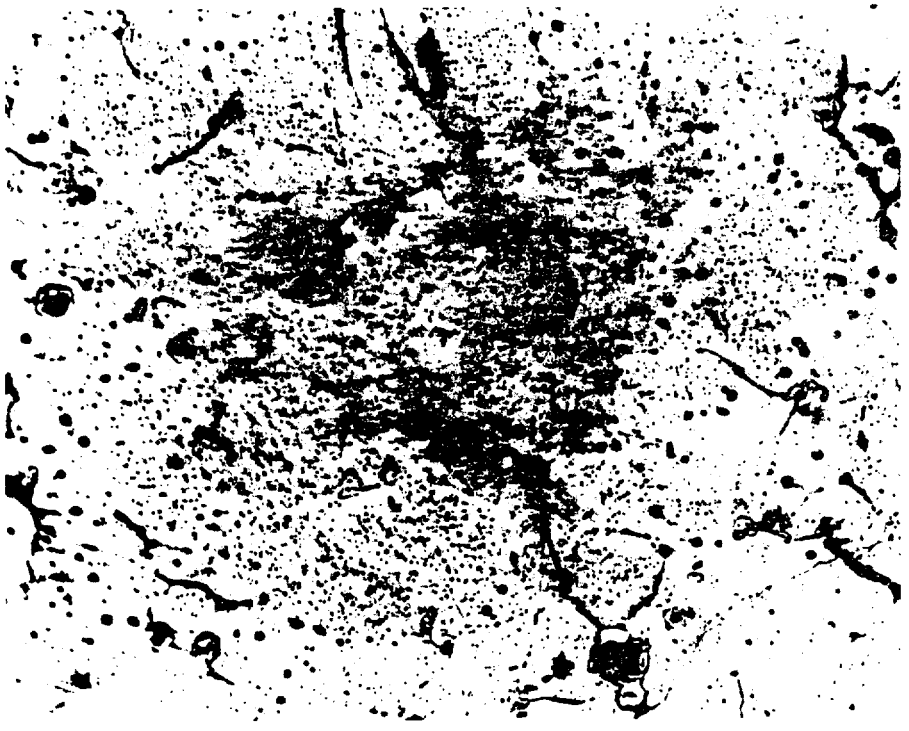

Fig. IV-32 Very Small Fuel Particles and Large Islands with Cored Area, Element E-65, Sample R-155 Etch-Polish-2 for 16 seconds, 500 x Magnification.

1256044

3.2 Fuel Element Cladding

Several samples (shown in Figures IV-33 and IV-34 and described in Table VIII) from fuel elements E-65, E-84, and E-151 were taken to evaluate the effect of the destructive test on the cladding. The components under investigation were the cladding base metal (Hastelloy-N), the chromized layer on both walls of the base metal, and the hydrogen barrier material located on the inside wall of the cladding. The properties and effects under consideration included grain size, precipitation and age hardening effects, fracture mechanisms, and various microstructure changes.

3.21 Grain Size

The following cladding samples were examined to determine any changes in grain size, A-175, A-173A, A-173B, A-165A, and A-165C. It appeared that no increase in grain size took place between the cold end and the hot end of elements E-84 (Figures IV-35, IV-36, and IV-37) and E-65 (Figures IV-38 and IV-39). It also appears from these figures that there is an inhomogeneous grain size which is most likely a result of fabrication techniques.

3.22 Precipitation and Age Hardening Effects

A study of microstructure and hardness was conducted to evaluate the possible precipitation and hardness effects which might have taken place in the cladding due to the destructive test. An estimate of the precipitation effects in samples from the cladding of elements E-65 and E-84 indicated that the cladding taken from the hot portion of E-65 exhibited a higher density of second phase particles (Figure IV-39) than did a cooler portion of the element (Figure IV-38). Element E-84 showed no quantative difference in particle density between the cold and hot portions of the element shown in Figures IV-35, IV-36, and IV-37. Two possibilities for the above mentioned situation are: (1) etching differences during the metallographic processing (the structure was etched longer in Figures IV-38 and IV-39 and appears darker and more dense than do the particles in Figues IV-35, IV-36, and IV-37) or, (2) the actual heat generated by element E-65 is greater than by E-84 which is quite possible due to their relative positions in the core.

1256045

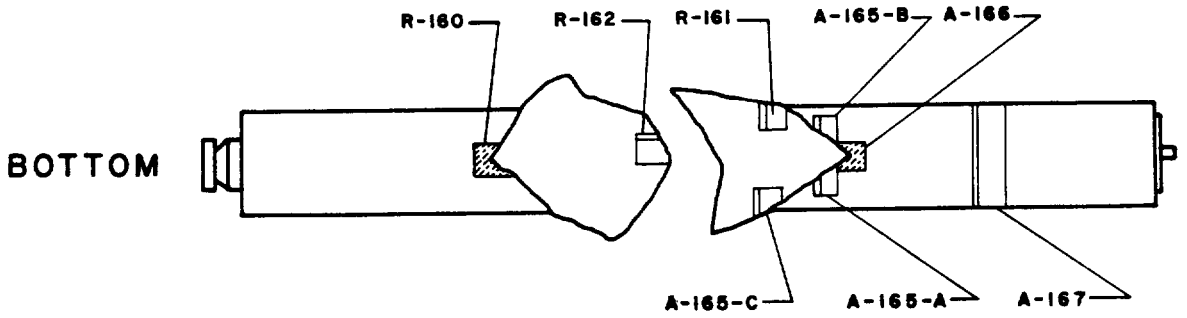

NOTES:

1. DRAWING NOT TO SCALE.
2. DOUBLE LINES ON SPECIMENS INDICATE THE MOUNTED SURFACE.

Fig. IV-33 Element E-65 Cladding Samples.

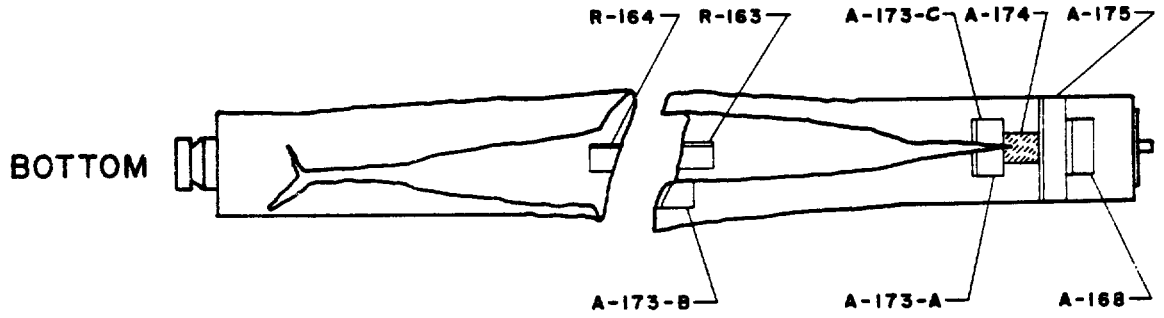

NOTES:

1. DRAWING NOT TO SCALE.
2. DOUBLE LINES ON SPECIMENS INDICATE THE MOUNTED SURFACE.

Fig. IV-34 Element E-84 Cladding Samples.

1256046

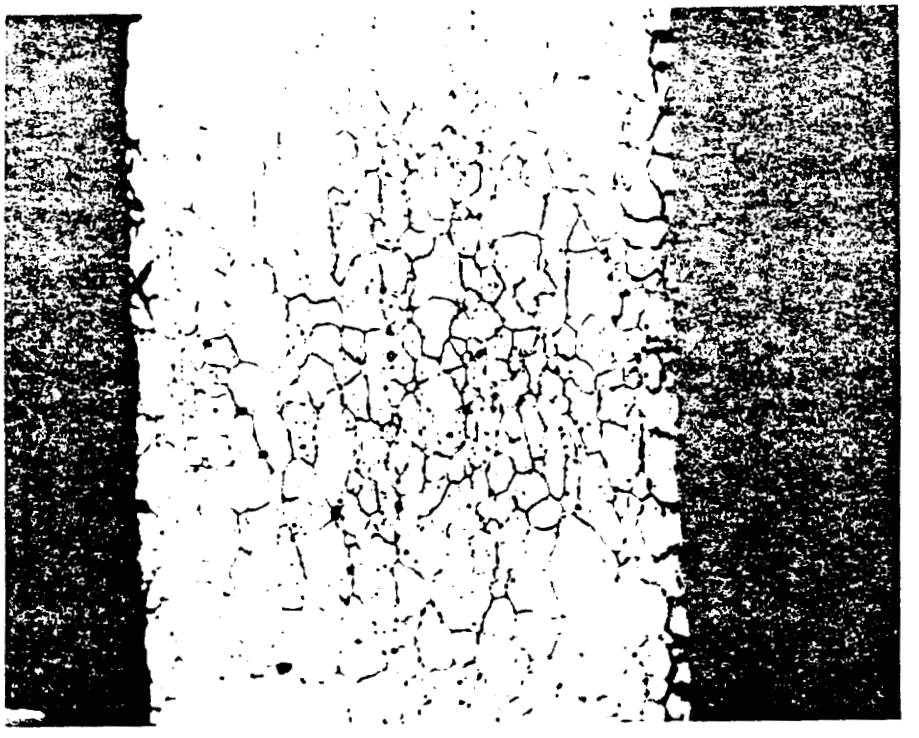

Fig. IV-35 Cladding Grain Structure at the Cold End of the Element, Element E-84, Sample A-175, Shantz Etch for 10 seconds, 250 x Magnification.

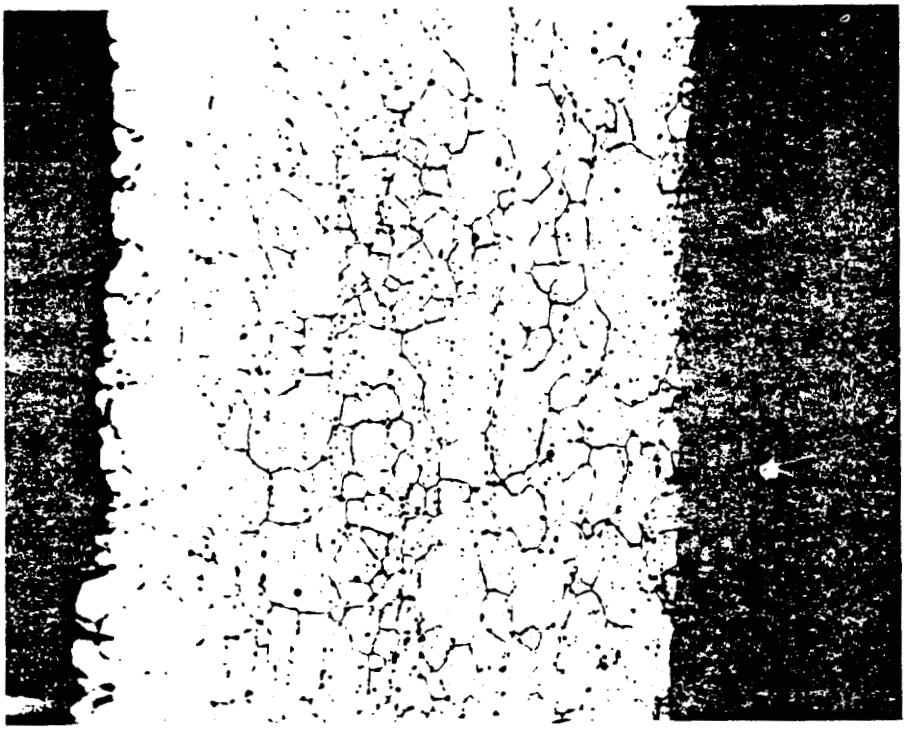

Fig. IV-36 Cladding Grain Structure at the Crack Termination Region of the Element, Element E-84, Sample A-173A, Shantz Etch for 10 seconds, 250 x Magnification.

1256047

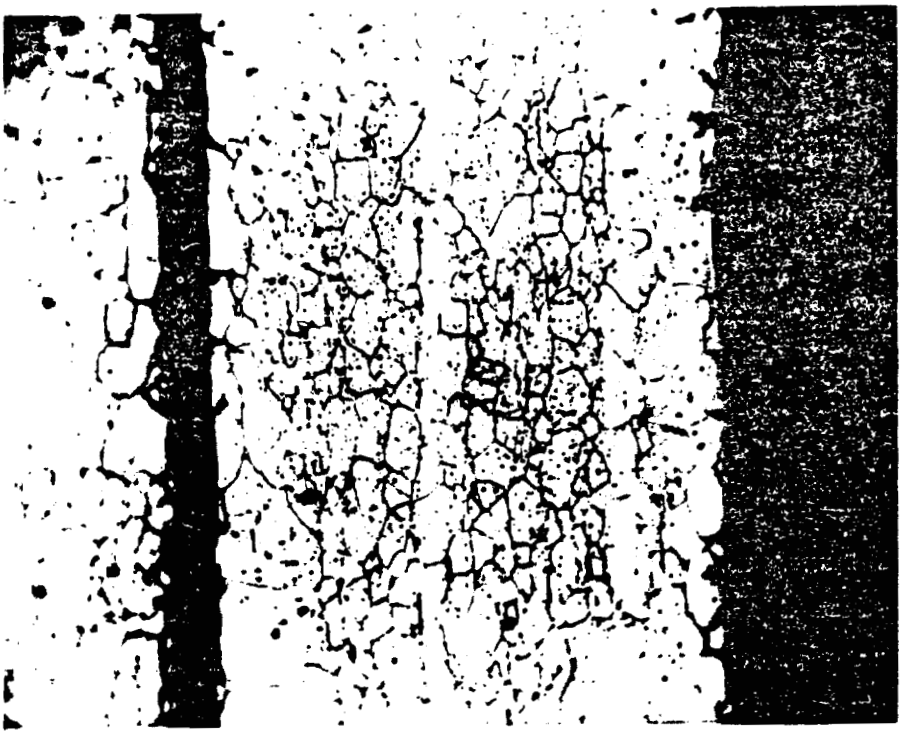

Fig. IV-37 Cladding Grain Structure at the Hot End of the Element, Element E-84, Sample A-173B, Shantz Etch for 10 seconds, 250 x Magnification.

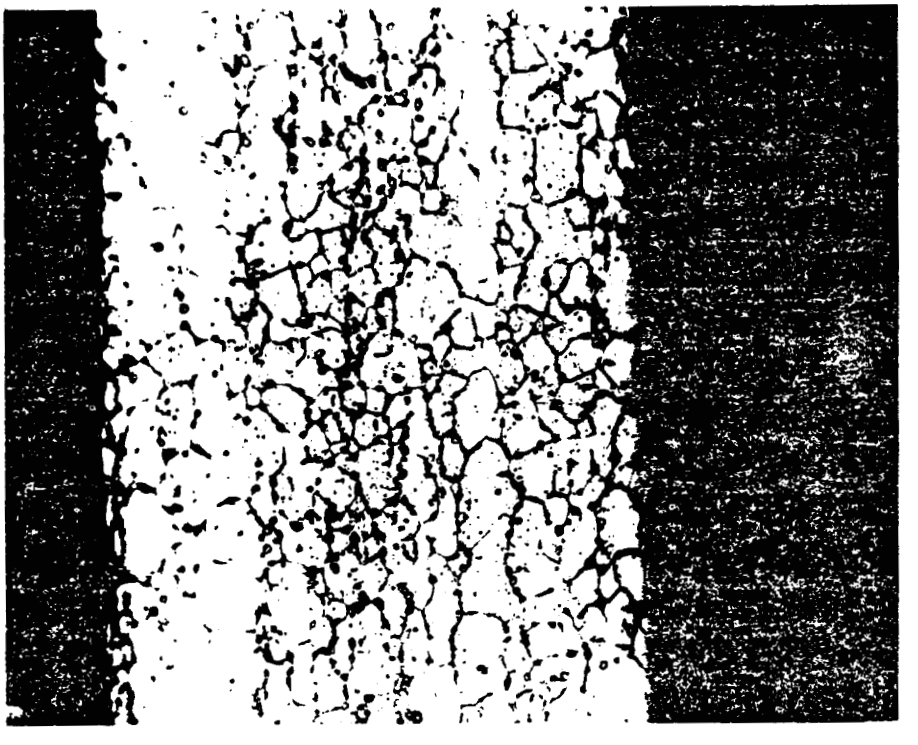

Fig. IV-38 Cladding Grain Structure at the Cold End of the Element, Element E-65, Sample A-165A, Shantz Etch for 15 seconds, 250 x Magnification.

1256048

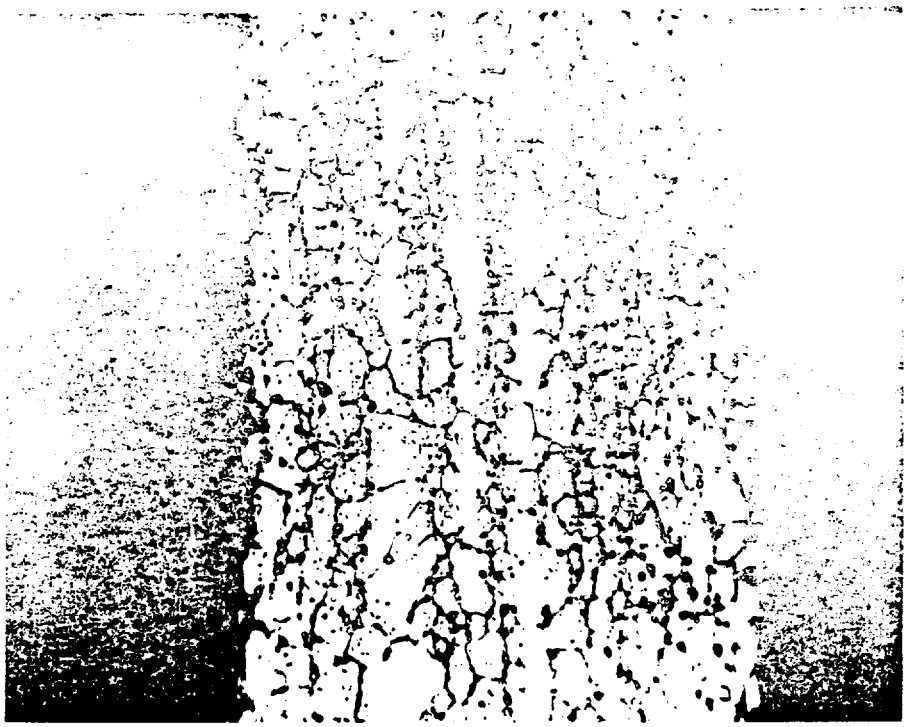

Fig. IV-39 Cladding Grain Structure at the Hot End of the Element, Element E-65, Sample A-165C, Shantz Etch for 15 seconds, 250 x Magnification.

TABLE XI

CLADDING MICROHARDNESS

Sample	Knoop Hardness Number (1 kg. Load) Tested Area			
	Cladding, Wall		Weld, Wall	
Cladding (E-84)	ID	OD	ID	OD
A-175	271	279	374	314
A-173 A	311	308	425	356
A-173 B	326	339	370	342
R-163	317	279	No weld present	
Claddding (E-65)				
R-167	297	294		
A-165 A	329	297	363	374
A-165 C	320	323	367	374
R-161	262	247	No weld present	

All hardness numbers listed are an average of three indentations for cladding, and two indentations for cladding welds.

1256049

A review of the cladding hardness data given in Table XI indicates a hardness increases in both elements E-65 and E-84 from the cold end to the hot end with the inside wall generally harder that the outside wall from higher temperature inside. It should also be noted that all hardness numbers in this table are an average of three indentations for cladding and two indentations for cladding welds. The hardness data also appears to indicate that the cladding of elements E-65 and E-84 were both exposed to nearly equivalent temperatures.

3.23 Cladding Failure

Cladding samples from the two fuel elements E-65 (R-162) and E-84 (R-163) were examined to correlate the reduction in thickness at the failed edge with the temperature at the time of failure. The sources of both samples are from the hot ends of their respective fuel elements as shown in Figures IV-33 and IV-34. Figures IV-40, IV-41, IV-42, and IV-43 were used to determine the reduction in thickness which was found to be 51 percent in element E-65 (R-162) and 33 percent in element E-84 (R-163). These reductions could, according to McCoy[8], indicate temperatures of 1250°F for element E-65 (R-162) and 1450°F for element E-84 (R-163) or temperatures of 1100°F for element E-65 and 1050-1350°F for E-84 according to Swindeman[9]. A comparison of the grain structure at the failed edges of the two samples as shown in Figures IV-41 and IV-43 indicates that element E-84 may have failed at a lower temperature than E-65. Intergranular cracking is indicative of failure at elevated temperatures and transgranular cracking indicates low temperature failure. Sample R-162 (E-65) failed by intergranular cracking (Figure IV-41) and R-163 (E-84) failed by transgranular cracking (Figure IV-43). Swindeman[9] further indicates that Hastelloy-N fails transgranularly at temperatures below 1000°F and intergranularly above 1000°F. A complicating factor in this analysis may be the high speed at which the cladding failed. This could possibly result in transgranular cracking at temperatures in excess of 1000°F. Figures IV-44 and IV-45 show that the cladding failed initially in the high temperature region of the fuel cladding and progressed to and along the welded seam to the colder end of the element.

1256050

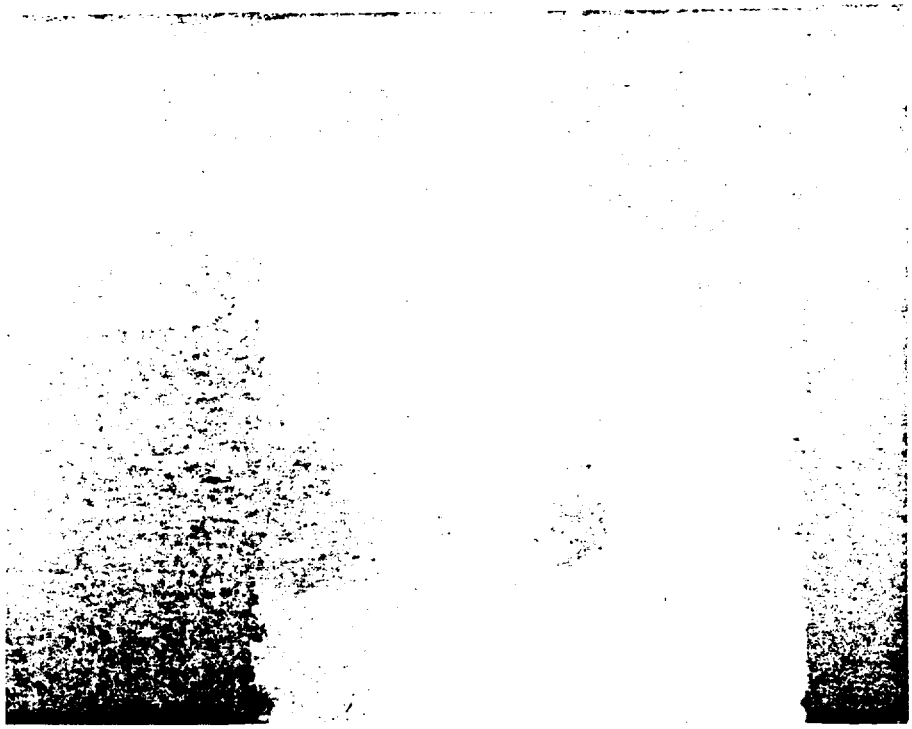

Fig. IV-40 Unfailed Cladding, Element E-65, Sample R-162 as Polished, 250 x Magnification.

Fig. IV-41 Failed Cladding, Element E-65, Sample R-162, Schantz Etch, 250 x Magnification.

1256051

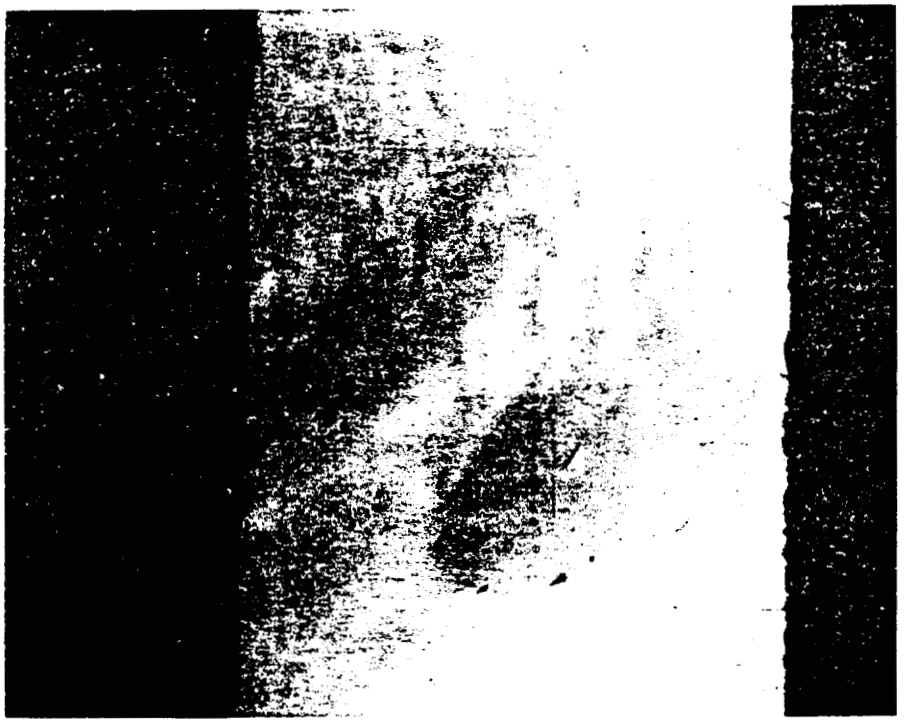

Fig. IV-42 Unfailed Cladding, Element E-84, Sample R-163, as Polished, 250 x Magnification.

Fig. IV-43 Failed Cladding, Element E-84, Sample R-163, Shantz Etch, 250 x Magnification.

1256052

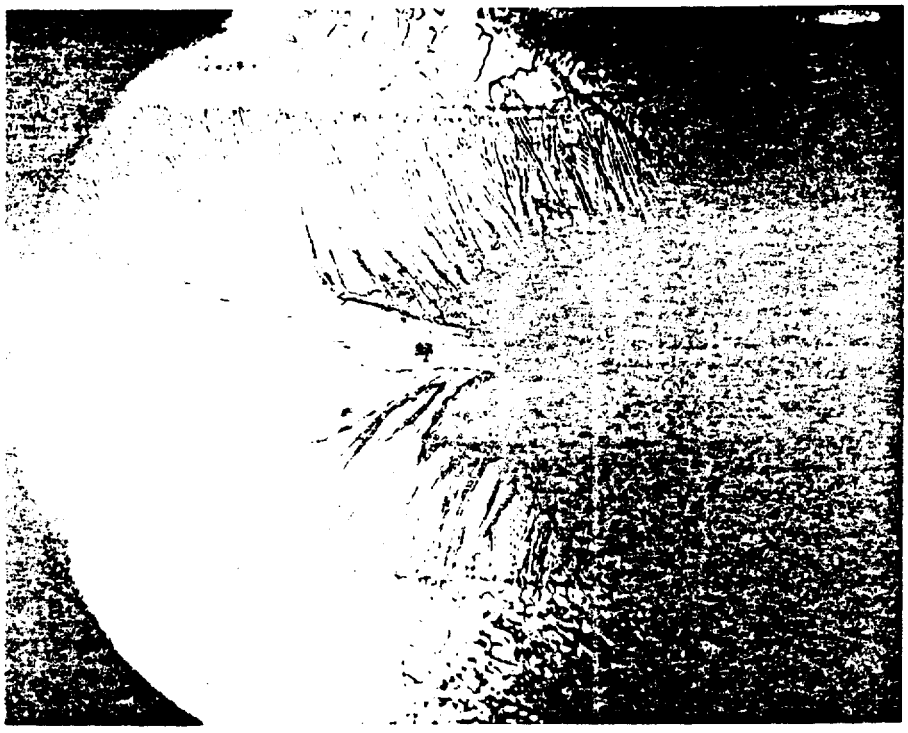

Fig. IV-44 Crack Termination in Weld, Element E-65, Sample A-166, Shantz Etch, 50 x Magnification.

Fig. IV-45 Crack Termination in Weld, Element E-84, Sample A-174, Shantz Etch, 50 x Magnification.

1256053

3.24 Chromized Layer

An investigation of the chromized layer on the cladding indicates a varying deposit thickness and possibly varying degrees of inter-action with the Hastelloy-N. The chromized layer is shown in Figures IV-46, IV-47, and IV-48 for samples R-161, R-162, and R-163 which were from the hot portions of elements E-65 and E-84. Figures IV-35, IV-36, IV-37, IV-38 and IV-39 should provide a profile of the effect of heat on the chromized layer but do not show any progressive differences. A comparison of Figures IV-47 and IV-48 with Figures IV-35 through IV-39 indicates that in the latter five structures the chromized layer reacted with the Hastelloy-N and is not readily identifiable in the photomicrographs. To determine the presence of absence of this interaction, samples R-161, A-165A, A-165C, A-167, A-173A, A-173B, and A-175 were analyzed by electron microprobe. The analysis did not indicate the outside chrome layer to be significantly higher at either the hot or cold ends.

3.3 Reactor Vessel Wall

The reactor vessel wall was also sampled and examined metallographically. Figures IV-49 and IV-50 show the wall in the interior and at the fracture edge respectively. Figure IV-49 shows the interior of the wall to be in relatively deformed condition. Figure IV-50 shows the failure to have taken place in a transgranular manner which would be expected of metal in an initially deformed condition.

Fig. IV-46 Chromized Layer on the Walls, Element E-65, Sample R-162, Shantz Etch, 250 x Magnification.

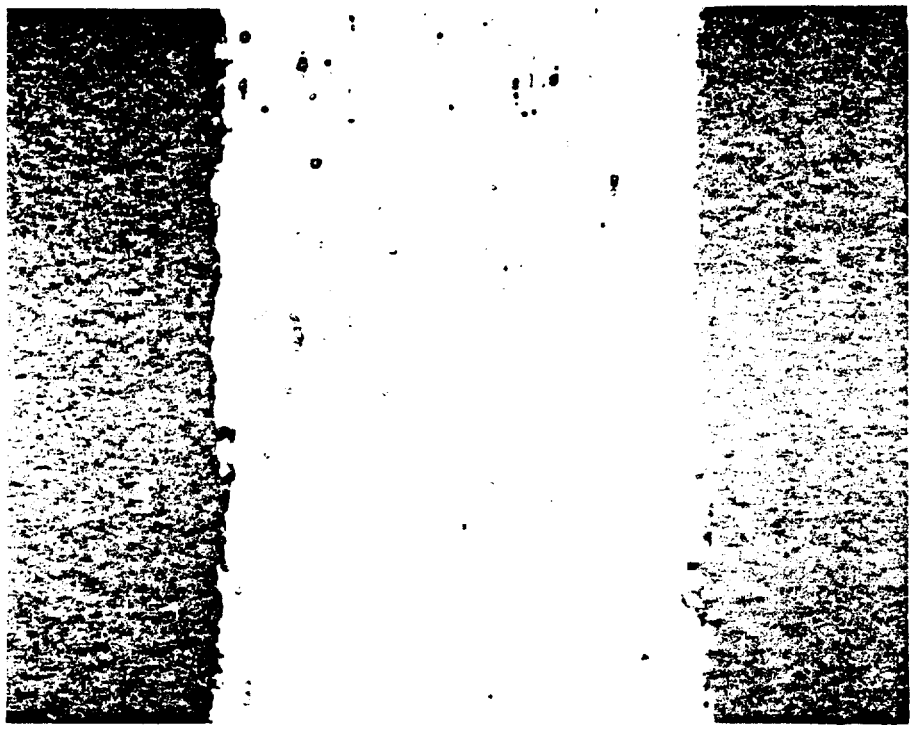

Fig. IV-47 Chromized Layer on the Walls, Element E-65, Sample R-162, Shantz Etch, 250 x Magnification.

1256055

Fig. IV-48 Chromized Layer on the Walls, Element E-84, Sample R-163, Shantz Etch, 250 x Magnification.

Fig. IV-49 Reactor Vessel Wall, Typical, Sample R-178, 10% Oxalic Etchant, 500 x Magnification.

1256056

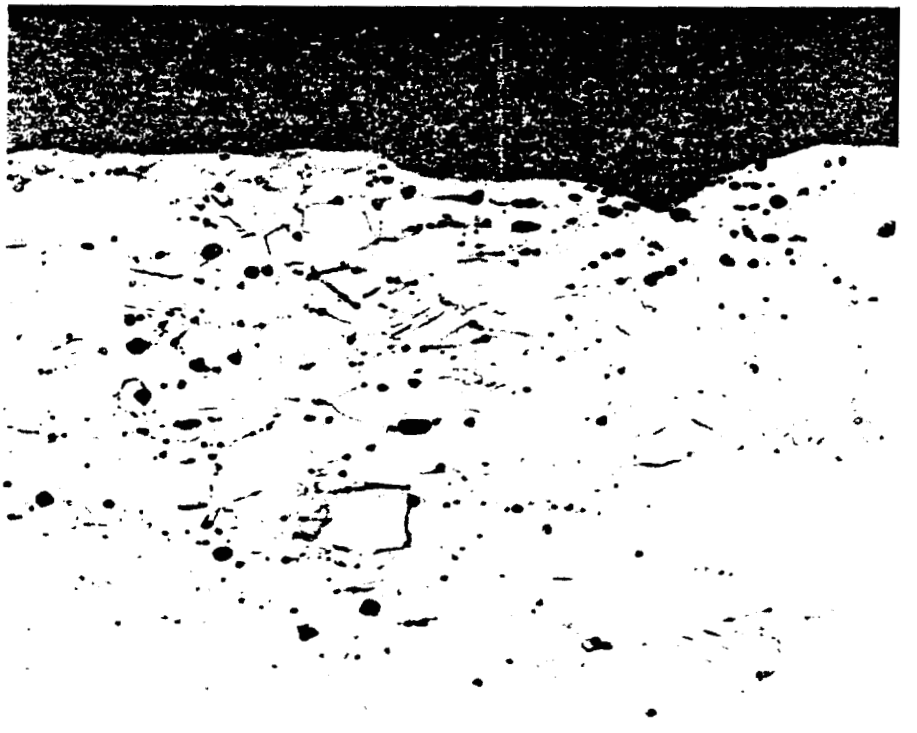

Fig. IV-50 Reactor Vessel Wall, Failed Edge, Sample R-178, 10% Oxalic Etchant, 500 x Magnification.

1256057

V. CONCLUSION

The objectives of the post destructive test examination of the SNAPTRAN 2/10A-3 fuel and reactor components were primarily related to reactor safety. The examination was intended to define the physical condition of the reactor following the destructive power excursion and supply information which would aid in understanding the nature of the reactor disassembly process by providing supplemental data associated with the nuclear and mechanical energy release. The general conclusions which can be drawn from the post-test examination of the fuel and reactor components are:

1. The dispersal of the reactor fuel and components resulting from the destructive test was less than anticipated. Although all 37 fuel elements were ruptured and broken, only 0.2 wt.% of the fuel was reduced to less than 150 microns size and essentially the entire core was retained in the environmental tank. Radiation levels 24 hours after the test were 3 rem/hr at the edge of the environmental tank with the water drained.

2. Detailed examination of the fuel indicated that the overall hydrogen release from the zirconium hydride was approximately 15% of the total or about 140 gms. The fission product analysis showed a higher flux toward the center of the core which was also confirmed by the radial and longitudinal flux profile curves from the activation analyses. The activation analysis flux shapes, both axially and radially, were also in good agreement with the spatial flux as determined by other means during the destructive test. Three distinct phases, epsilon. delta, and gamma were present in the grain structure with possible evidence of an alpha or beta phase. The various phase changes indicated that a minimum peak temperature of 1290°F was reached during the test. Fuel cracking at the grain boundries further indicated that the peak temperature

attained was probably in excess of 1740°F. An examination of the failed edges of the fuel cladding suggests that the clad temperature was probably in excess of 1000°F at the time of failure.

1256059

REFERENCES

1. W. E. Kessler, G. F. Brockett, O. L. Cordes, G. A. Dinneen, and R. D. Fletcher, "SNAPTRAN 2/10A-3 Destructive Test Results", IDO-17019 (September, 1964).

2. Beck, R. L., "Zirconium-Hydrogen Phase System", Trans., ASM, Vol. 55, (1962).

3. Shoop, D. T. , "Metallographic Preparation of Zirconium-Hydride", NAA-SR-MEMO-10145, (1964).

4. Filer, E. W., Rau, R. C., and Tholke, W. H., "A Metal Hydride System", GE-ANPO, APEX-444 (1958).

5. Vetrano, J. B., and Atkens, D. F., "The Zirconium-Hydrogen System", Nuclear Met. VII, AIME, Inst. of Metals Div. (1960).

6. Vaughan, D. A. and Bridge, J. R., "High Temperature X-Ray Diffraction Investigation of the Zr-H System", J. of Metals Trans. Vol. 8, (1956).

7. Beck, R. L., "Thermophysical Properties of Zirconium-Hydride", Trans. ASM, Vol. 55, (1962).

8. McCoy, H. E., "Influence of Several Metallurgical Variables on the Tensile Properties of Hastelloy-N", ORNL-3661, (1964).

9. Swindeman, R. W., "The Mechanical Properties of INOR-8", ORNL-2780, (1961).

1256060

RECEIVED
PHILLIPS PETROLEUM CO.
JUN 29 1965
NRTS
TECHNICAL LIBRARY

PHILLIPS
PETROLEUM
COMPANY

PHILLIPS
66

1256061